american physiological society

JNP JOURNAL OF NEUROPHYSIOLOGY

J Neurophysiol 134: 1785–1803, 2025.
First published October 8, 2025; doi:10.1152/jn.00518.2024

RESEARCH ARTICLE

Sensory Processing

Visual context affects the perceived timing of tactile sensations elicited through intracortical microstimulation: a case study of two participants

Isabelle A. Rosenthal,[1,2,3] Luke Bashford,[1,2,4] David Bjånes,[1,2] Kelsie Pejsa,[1,2] Brian Lee,[1,5,6] Charles Liu,[1,5,6,7] and Richard A. Andersen[1,2]

[1]*Division of Biology and Biological Engineering, California Institute of Technology, Pasadena, California, United States;* [2]*T&C Chen Brain-machine Interface Center, California Institute of Technology, Pasadena, California, United States;* [3]*Institute of Bioelectronic Medicine, Feinstein Institutes for Medical Research, Manhasset, New York, United States;* [4]*Faculty of Medical Sciences, Newcastle University, Newcastle upon Tyne, United Kingdom;* [5]*Department of Neurological Surgery, Keck School of Medicine of USC, Los Angeles, California, United States;* [6]*USC Neurorestoration Center, Keck School of Medicine of USC, Los Angeles, California, United States; and* [7]*Rancho Los Amigos National Rehabilitation Center, Downey, California, United States*

Abstract

Intracortical microstimulation (ICMS) is a technique to provide tactile sensations for a somatosensory brain-machine interface (BMI). A viable BMI must function within the rich, multisensory environment of the real world, but how ICMS is integrated with other sensory modalities is poorly understood. To investigate how ICMS percepts are integrated with visual information, ICMS and visual stimuli were delivered at varying times relative to one another. Both visual context and ICMS current amplitude were found to bias the qualitative experience of ICMS. In two tetraplegic participants, ICMS and visual stimuli were more likely to be experienced as occurring simultaneously in a realistic visual condition compared with an abstract one, demonstrating an effect of visual context on the temporal binding window. The peak of the temporal binding window varied but was consistently offset from zero, suggesting that multisensory integration with ICMS can suffer from temporal misalignment. Recordings from primary somatosensory cortex (S1) during catch trials where visual stimuli were delivered without ICMS demonstrated that S1 represents visual information related to ICMS across visual contexts. This study was a part of a clinical trial (NCT01964261).

NEW & NOTEWORTHY Little is known about how the brain integrates tactile sensations elicited through intracortical microstimulation (ICMS) with visual information. This work investigates how visual cues affect the perception of tactile sensations from ICMS in two human participants. The results suggest that visual context can influence the perceived timing and the qualitative nature of artificial sensations, which is directly relevant to the implementation of a viable brain-machine interface (BMI) for individuals with tactile impairments.

brain-machine interfaces; intracortical microstimulation; multisensory integration; somatosensation; vision

INTRODUCTION

Tactile sensation is highly important for executing dexterous, adaptable movements (1–5) and providing a sense of embodiment (6–8). In cases of spinal cord injury (SCI), motor and somatosensory abilities are impaired or fully lost below the level of the injury. Brain-machine interfaces (BMIs) provide a potential method to restore these abilities by decoding motor intentions from neural activity (9–11), and by using intracortical microstimulation (ICMS) in primary somatosensory cortex (S1) to elicit artificial tactile sensations (12, 13).

Motor BMIs have become more accurate and sophisticated over the past 15 years (10, 14–16). In contrast, broadly viable somatosensory BMIs remain at the proof-of-concept stage (17), although some principles mapping the relationship between ICMS and sensations have emerged. A higher ICMS current amplitude elicits sensations more often than a lower current amplitude, and the sensations tend to be rated as

Correspondence: I. A. Rosenthal (isabellearosenthal@gmail.com).
Submitted 1 November 2024 / Revised 26 November 2024 / Accepted 11 September 2025

more intense (12, 13, 18, 19). The perceived location of elicited sensations reflects the topographic organization of S1 according to where the stimulation microelectrode arrays are implanted (12, 13). However, it remains poorly understood how to achieve reliable, replicable sensations with controllable qualia because experiences of ICMS can vary widely across electrodes, participants, and experiments, even when stimulation parameters are kept constant (12, 13, 20).

A somatosensory BMI implemented in the real world will necessitate ICMS being processed by the brain as part of a complex multisensory environment (21, 22). To this end, understanding how ICMS is combined with other sensory inputs to produce perceptual experiences is essential. It has been shown in amputees that peripheral nerve stimulation and visual information relating to prosthetic control can be integrated in a statistically optimal fashion (22, 23). Although this finding has yet to be shown using ICMS, reaction time studies have shown that artificial tactile sensations from ICMS can be slower compared with real tactile inputs or visual stimuli (18, 24–26). However, although relative processing speeds between sensory modalities have been investigated, the dynamics of how they are integrated together are still unclear.

Given that visual and tactile stimuli are often paired together in the real world, the characteristics of the temporal binding window, or the period of time in which two stimuli are perceived as occurring simultaneously, need to be mapped out with respect to ICMS and visual stimuli. It has been shown that the optimal timing needed to perceive peripheral nerve stimulation and visual stimuli as simultaneous is not always the same; peripheral stimulation in the leg must occur earlier than in the hand relative to visual stimuli to achieve optimal synchronicity (27). Yet, the temporal binding window between ICMS and vision remains unclear, and it is unknown what timings would be optimal to perceive ICMS and a visual cue as simultaneous.

In addition to timing considerations, it is also possible that vision can affect the qualia of ICMS-elicited sensations. Some work in lower limb amputees has shown that visual information can bias the localization of sensations elicited through peripheral nerve stimulation (28). However, there has been little research on the potential effects of visual context on the neural processing and perceptual results of ICMS.

In this case study, we explore the behavioral and neural results of pairing ICMS and visual stimuli in two tetraplegic patients implanted with microelectrode arrays in primary somatosensory cortex (S1) (Fig. 1*A*). To understand the importance of biologically relevant visual information to the perception of ICMS sensations, two visual conditions are used which differ in their level of realism (Fig. 1*C*). The visual stimuli are presented at varying temporal offsets relative to ICMS to better characterize the temporal binding window between ICMS and vision (Fig. 1*B*), and S1 recordings are examined during catch trials to assess the neural response to visual information related to ICMS. We find evidence that both visual context and ICMS current amplitude are capable of biasing qualitative aspects of ICMS-elicited sensations, and that the temporal binding window changes based on the biological relevance of visual context. In addition, the point of peak simultaneity (PSS) of ICMS and vision varied substantially between the two participants, but was offset from zero in both, indicating an imperfect temporal alignment between ICMS and visual stimuli.

Finally, we show that S1 represents information from visual stimuli relevant to ICMS in a context-independent manner. This case study lays the groundwork for the implementation of BMIs using ICMS to elicit naturalistic sensations that can be temporally and perceptually integrated with the real-world environment.

METHODS

Participants

As part of a brain-machine interface (BMI) clinical trial (NCT01964261) involving intracortical recording and stimulation, two tetraplegic participants (both male, aged 33 and 39) with C5-level spinal cord injuries were recruited and provided written informed consent. Participants were included in this study based on a cervical spinal cord injury, age (22–65 yr), and impairment of motor and sensory function in the hand. The microelectrode array implants of *participant 1* (*P1*) were placed in three locations in the left hemisphere: the supramarginal gyrus (SMG), ventral premotor cortex (PMv), and primary somatosensory cortex (S1). At the first experimental session, *P1* was 5.5 yr postimplant and 7 yr postinjury. *Participant 2* (*P2*) was implanted with microelectrode arrays in five locations on the left hemisphere: SMG, PMv, primary motor cortex (M1), anterior intraparietal area (AIP), and S1. At the first experimental session, *P2* was 1 yr postimplant and 3.5 yr postinjury.

In total, two S1 arrays were implanted in each participant (Fig. 1*A*). These arrays were 1.5 mm sputtered iridium oxide film (SIROF)-tipped microelectrode arrays (Blackrock Neurotech, Salt Lake City, UT). *P1*'s arrays were 48-channel; *P2*'s arrays were 64-channel. Given the constraints of implanting arrays on the surface of cortex and the anatomy of S1, it is likely the S1 microelectrode arrays in both participants are located in Brodmann area 1 (BA 1) (29). Implant locations were determined based on functional magnetic resonance imaging (fMRI) motor and sensory localizer tasks. Additional information on the surgical methodology is available in the study by Armenta Salas et al. (12). Both participants remained in the study for the entire duration of the experiment.

All procedures were approved by the Institutional Review Boards (IRB) of the California Institute of Technology, University of Southern California, and Rancho Los Amigos National Rehabilitation Hospital.

Experimental Paradigm

Two task conditions were tested in a block format with both *P1* and *P2*: a realistic condition and an abstract condition (Fig. 1, *B* and *C*). The order of presentation of these blocks alternated so no condition was consistently presented first. In addition, a baseline condition was tested in *P1*, which always occurred before the other two conditions (Table 1). All ICMS across conditions occurred on the same single electrode within each participant, at 300 Hz for 0.5 s, with a pulse-width of 200 μs and an interphase of 60 μs. For each participant, the stimulating electrode was selected for high reliability in eliciting tactile percepts based on earlier ICMS experiments. The current amplitude of ICMS in all conditions was varied with the trial (30, 60, 100 μA). As higher

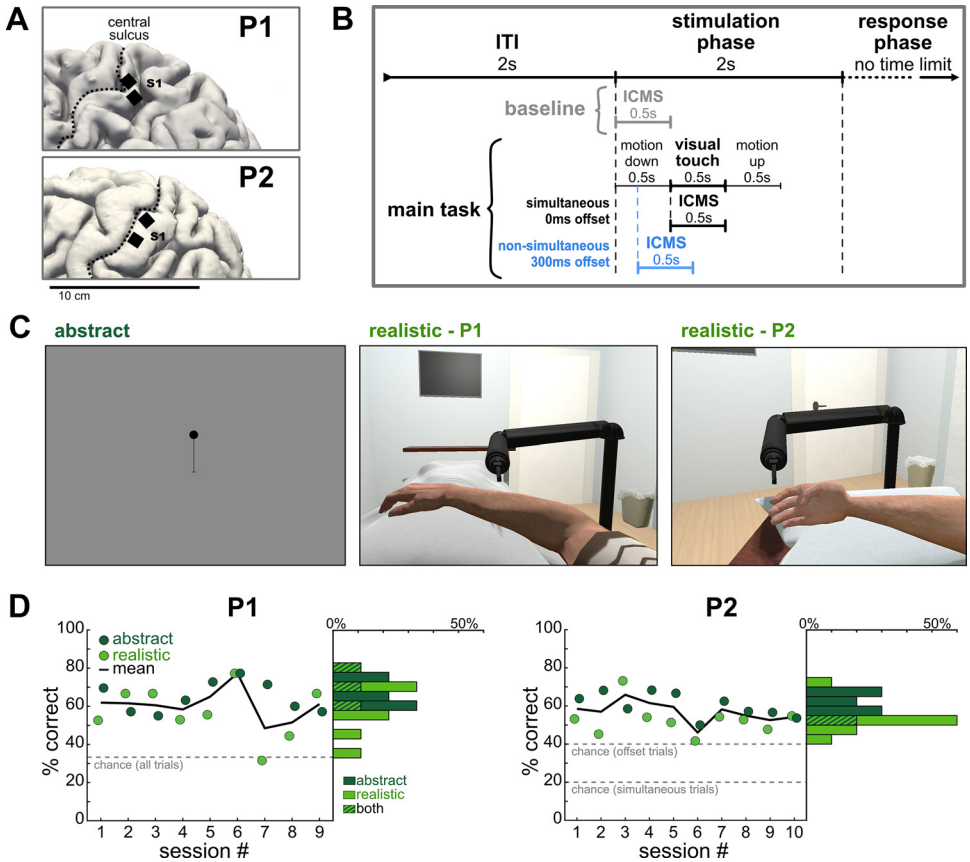

Figure 1. Experimental methods and paradigm. *A:* microelectrode array implant locations ($n = 2$), visualized using MRI on the cortical surface of each participant's left hemisphere. *B*: task time course. In the baseline, only intracortical microstimulation (ICMS) was delivered. In the main task (either abstract or realistic), a visual cue was temporally linked to the ICMS at a given offset ranging between −300 and 300 ms); 300 ms offset is depicted. *C*: sample frames from visual cues. In the abstract condition, the dot moved down to contact the end of the line. In the realistic condition, the robotic arm moved down to contact the virtual body: either the forearm (*P1*) or the index finger (*P2*). See Supplemental Videos S1, S2, and S3. *D*: scatter plot depicts behavioral accuracy across experimental sessions within each participant, quantified as the percentage of the trials where the participant reported a sensation, in which the participant's reported order of stimuli (either vision first, ICMS first, or simultaneous) matched the ground truth stimulus order. For instance, if the participant stated that ICMS occurred first, and the ICMS occurred any time before the visual stimulus, this would count as a correct trial. If the participant reported simultaneous stimuli, this was only counted as correct if the stimuli were delivered with an offset of 0 s. *P1*: chance = 33.3% as all trial types (vision first, ICMS first, simultaneous) were evenly presented. *P2*: $\text{chance}_{\text{simultaneous}} = 40\%$, $\text{chance}_{\text{offset}} = 20\%$ as trial types were unevenly sampled (see METHODS). Histograms to the right of the scatter indicate behavioral accuracy binned across sessions. The average number of trials felt per session in realistic runs was 18.2 (SD = 1.9) for *P1* and 39.7 (SD = 4.1) for *P2*; in abstract runs the average was 19.7 (SD = 3.2) for *P1* and 41.6 (SD = 5.8) for *P2*. Black line = mean across abstract and realistic runs.

current amplitudes generally elicit more intense sensations (Fig. 2*A* and Fig. 3*A*), these current amplitudes were chosen to provide a range of sensation intensities while not exceeding safe levels of stimulation.

In the baseline condition (18 trials per block), *P1* viewed grids of the upper body and hand on a gray background that remained static throughout the task. Each trial contained a 2-s intertrial interval (ITI), a 2-s stimulation phase, and a response phase without a time limit. In each trial, 0.5 s of ICMS was delivered immediately upon entering the stimulation phase, at one of the three current amplitudes that were pseudo-randomly sampled in the block (5 trials each). The baseline also

Table 1. *Differences in the experimental paradigm between participants*

	P1	P2
Conditions tested in each block	Baseline (18 trials/block) Abstract (40 trials/block) Realistic (40 trials/block)	Abstract (64 trials/block) Realistic (64 trials/block)
Total sets of blocks collected	9 sets	10 sets
Time span of data collection	6 mo	3 mo
Virtual reality "touch" location	Arm	Index finger
Temporal offsets tested	−300, −150, 0, 150, 300 ms	−300, −225, −150, −75, 0, 75, 150, 225, 300 ms
Qualitative measures of ICMS	Collected each trial	Not collected each trial
Number of S1 channels recorded	96	128

ICMS, intracortical microstimulation; S1, primary somatosensory cortex.

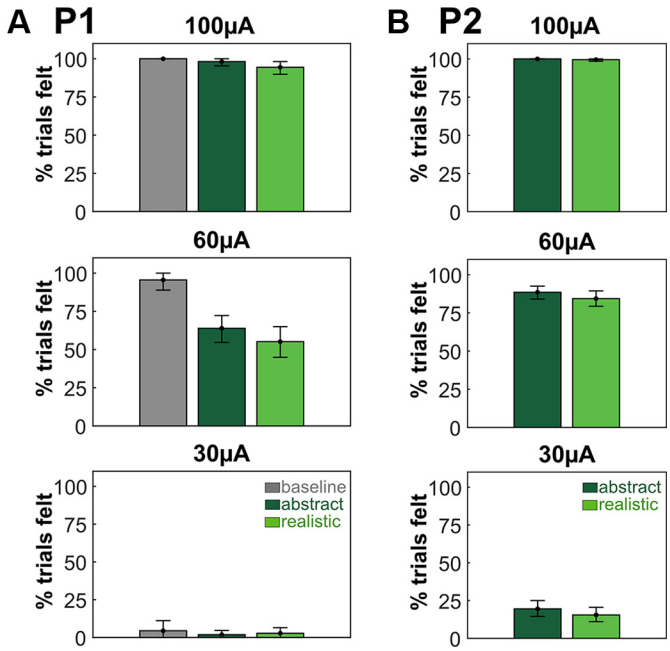

Figure 2. Tactile sensation rates within intracortical microstimulation (ICMS) amplitudes. *A*: percentage of trials eliciting a sensation across conditions and timing offsets in participant *P1*, sorted by ICMS current. Within realistic and abstract conditions, values are aggregated across timing offsets (see APPENDIX Fig. A1). Error bars represent 95% confidence intervals (CIs) assessed by bootstrapping values across 1,000 iterations sampling from trials with replacement. *B*: analysis identical to (*A*), using data from participant *P2*.

contained three catch trials where no stimulation was delivered. During the response phase, the participant was given an auditory cue (a beep) to verbally indicate whether or not he experienced a tactile sensation from ICMS. In the affirmative case he used the grids as references to indicate the sensation location. He also relayed the duration ("Short," "Medium," or "Long"), a qualitative descriptor of the sensation (free word choice), and the intensity (on a subjective scale).

During the realistic and abstract conditions tested in both participants, visual and ICMS cues were delivered at varying temporal offsets to one another. Participants were instructed to report if they felt an ICMS-elicited tactile sensation, and if so, the perceived temporal order of the stimuli—either stating that the visual stimulus came first, the ICMS stimulus came first, or they occurred simultaneously. Similar to the baseline condition, each trial contained a 2-s ITI, a 2-s stimulation/visual cue presentation phase, and a response phase without a time limit (Fig. 1*B*). The current amplitude of the ICMS stimulation was pseudo-randomly sampled (30, 60, 100 μA) and always delivered on the same single electrode within each participant.

In the abstract condition, the participants viewed a two-dimensional (2-D) black dot positioned at the top of a black line on a gray background (Fig. 1*C*, Supplemental Video S1). In the realistic condition, the virtual reality (VR) headset was used to give the participants a first-person perspective of a body with a size, gender, and posture reflecting their own body (Fig. 1*C*, Supplemental Videos S2 and S3), which was taken from the Microsoft Rocketbox Avatar Library (30) (Table 2, https://github.com/microsoft/Microsoft-Rocketbox/). In the VR environment, a virtual robotic, articulated arm with a narrow rod protruding from the end was positioned over *P1*'s virtual arm or *P2*'s virtual finger. *P1*'s forearm and *P2*'s index finger were selected as targets for a visually depicted touch to match the respective projected fields of the stimulated electrodes for each participant.

During the stimulation phase, both a visual and ICMS cue were delivered at some temporal offset from one another. In the realistic condition, the visual cue was the robotic arm performing a single tap of *P1*'s virtual arm or *P2*'s virtual finger, and in the abstract condition, it was the dot moving along the line to tap the base of the line (Fig. 1*C*, Supplemental Videos S1, S2, and S3). In both conditions, the virtual cue was composed of 0.5-s motion downward, 0.5-s contact ("visual touch"), and 0.5-s motion upward to the original position (Fig. 1*B*), such that the direction and magnitude of movement in the visual field were held constant across conditions.

Due to restricted experimental session time, slightly different experimental paradigms were conducted between *P1* and *P2* (Table 1). The temporal offsets between visual and ICMS cues tested with *P1* were [−300, −150, 0, 150, 300 ms]. The offsets tested with *P2* were [−300, −225, −150, −75, 0, 75, 150, 225, 300 ms]. In addition, after *P1*'s temporal order response in each trial where an ICMS sensation was elicited, he reported that sensation's anatomical location using a grid of the upper body and intensity, and a one-word descriptor for the sensation's qualitative nature. The qualitative descriptor was always solely generated by the participant and was not selected from any predefined list of words.

In 12 of the trials in a realistic or abstract block (*P1*: 40 trials per block total; *P2*: 64 trials), the visual and ICMS cues were presented simultaneously (0 ms). The range of timing offsets (−300 to 300 ms) was chosen based on previously established timings in the visuo-tactile multisensory integration literature, which indicates that a 300-ms delay is typically an easily noticeable offset between visual and tactile stimuli, whereas a 150-ms delay is typically the point of just-noticeable difference (27, 34–36). Visual contact occurred before ICMS began in 12 trials for *P1* and 24 trials for *P2* (6 trials per individual offset). Similarly, visual contact occurred after ICMS began in 12 trials for *P1* and 24 trials for *P2*. There were also four catch trials where the visual cue was delivered without ICMS. ICMS amplitudes (30, 60, 100 μA) were sampled evenly within timing conditions. Within conditions, trials were pseudo-randomly shuffled. The order of the realistic and abstract condition blocks was alternated across days, whereas ICMS amplitudes were shuffled randomly within blocks.

Nine sets of all three conditions were collected for *P1*; ten sets of the realistic and abstract conditions were collected for *P2*. During all conditions, visual stimuli were shown to the participants using a Vive Pro Eye virtual reality (VR) headset (HTC Corporation, Taoyuan City, Taiwan), which was programmed using Unity. Within each trial, participants were blinded to the ICMS current amplitude and, in the visual conditions, the timing offsets between visual and ICMS cues.

Data Collection

In total, nine sets of conditions were collected with *P1* on nine unique days over 6 mo (Table 1). Ten sets were collected with *P2* on six unique days over 3 mo. Neural data were recorded from the S1 microelectrode arrays using a Neural Biopotential Signal Processor as 30,000 Hz broadband

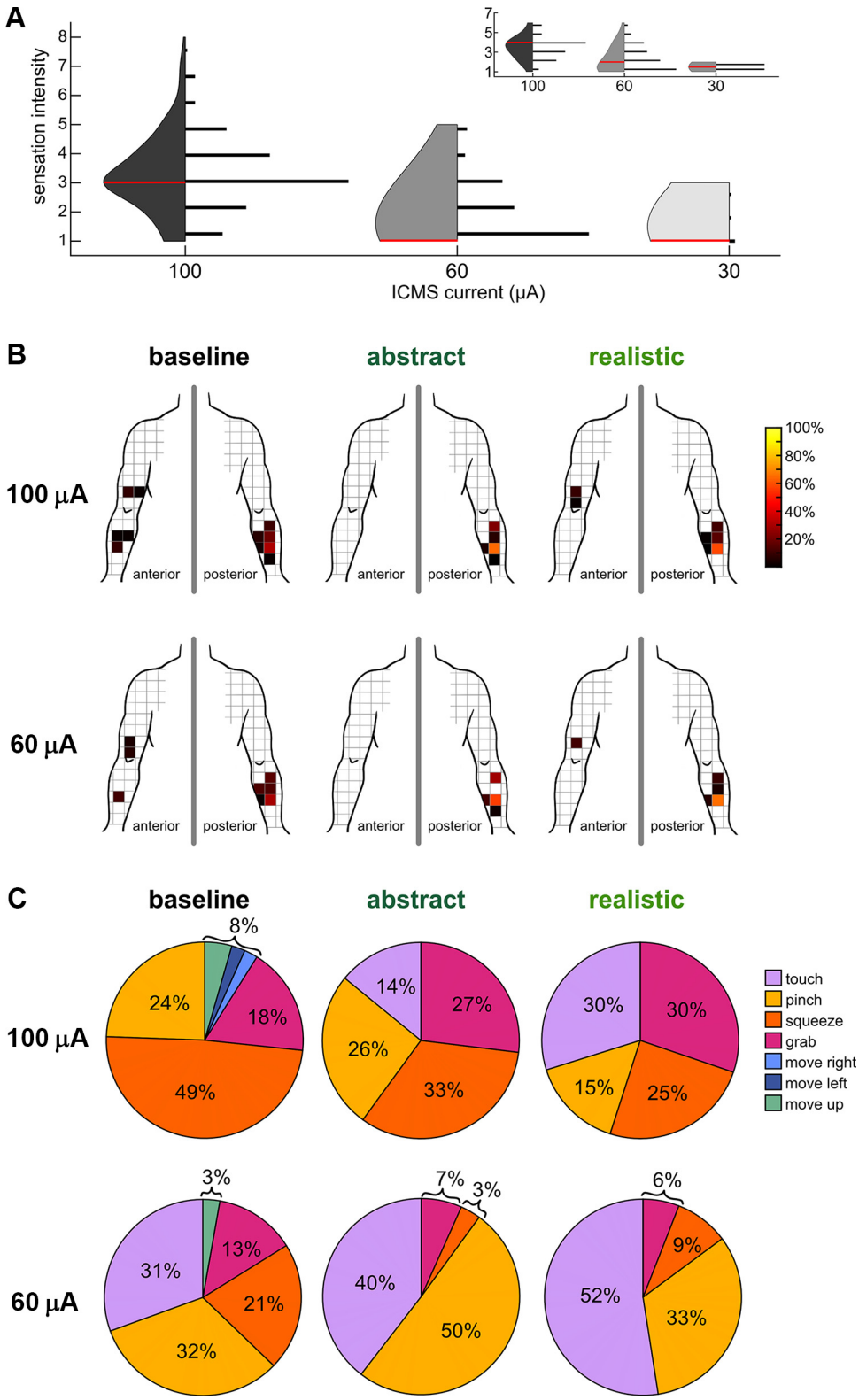

Figure 3. Qualia of intracortical microstimulation (ICMS)-elicited tactile percepts in *P1*. *A*: violin plot and histogram of reported sensation intensity separated by ICMS current and combined across abstract and realistic trials. Red line = median value. Histograms are to scale with the number of trials (n for 100 μA = 83, 60 μA = 67, 30 μA = 3 trials). *Inset*: sensation intensity for baseline trials, analysis identical to main figure (n for 100 μA = 45, 60 μA = 43, 30 μA = 2 trials). *B*: locations of elicited sensations by condition and ICMS amplitude. Each sensation's location was confined to one box in the grid of the arm. *C*: pie charts of sensation descriptors by condition and ICMS current amplitude. Only one word was used to describe each sensation. *Top* = 100 μA (baseline n = 45, abstract n = 106, realistic n = 102 trials). *Bottom* = 60 μA (baseline n = 43, abstract n = 69, realistic n = 59 trials).

signals, and a CereStim96 device was used to deliver ICMS in S1 (Table 2, Blackrock Neurotech, Salt Lake City, UT).

A central computer used custom MATLAB (Table 2, MathWorks, Natick, MA) code with synchronized ICMS and visual outputs, the latter of which were displayed with a virtual reality headset (Vive Pro Eye, HTC Corporation, Taoyuan City, Taiwan). Eyetracking data were collected in both participants using the built-in camera and software in the VR headset, as well as custom Unity code.

The size and range of motion of the VR animation across the visual field in the realistic condition was constructed to be as similar as possible to the abstract condition. Although

Table 2. *Key resources table*

Reagent or Resource	Source	Identifier
Deposited data		
Preprocessed study data	This paper	https://doi.org/10.5281/zenodo.15284113
Software and algorithms		
Analysis code	This paper	https://doi.org/10.5281/zenodo.15284865
MATLAB R2019b, RRID:SCR_001622	MathWorks	http://www.mathworks.com
Python rsatoolbox	Walther et al. (31); GitHub	https://github.com/rsagroup/rsatoolbox
MATLAB rsatoolbox	Nili et al. (32); GitHub	https://github.com/rsagroup/rsatoolbox_matlab
Unity	Unity Technologies	https://unity.com/
Microsoft Rocketbox Avatar Library	Gonzalez–Franco et al. (33); Microsoft; GitHub	https://github.com/microsoft/Microsoft-Rocketbox/
Other		
Neuroport System	Blackrock Neurotech	https://blackrockneurotech.com/

exact equivalence was impossible due to the freedom of movement of the participant's head in the realistic VR space, the first-person camera view was initialized in a position that maximally preserved similarities between conditions. The size and range of motion of the visual animations in the realistic and abstract conditions were built to be as equal as possible across conditions.

Latencies to stimulus delivery were calculated and compensated for, resulting in a negligibly small unintended temporal offset of ICMS occurring an average of 5 ms (SD = 2 ms) earlier than planned in *P1* runs, and 10 ms (SD = 6 ms) in *P2* runs, relative to visual outputs across sessions. This small variability in latencies was due to variable frame rate update times within the VR headset.

Data Preprocessing and Analysis

All analyses were performed using MATLAB R2019b (Table 2, MathWorks, Natick, MA) unless otherwise noted. Data from *P1*'s S1 arrays were passed through a 180-Hz notch filter to remove an electrical artifact that occurred throughout all recording sessions. Similarly, data from *P2*'s S1 arrays were passed through a 60-Hz notch filter and a 920-Hz notch filter to remove electrical artifacts which also occurred throughout all recording sessions. Multiunit firing rates were computed from each channel's broadband signals in 50-ms bins without spike sorting (37, 38), with a threshold of −3.5 times the noise root mean square (RMS) of the continuous signal voltage. These firing rates were aligned within each trial to the ICMS and visual stimuli presented. Firing rates were normalized within each run and each channel by calculating the mean resting firing rate across the entire 2-s ITI period, and dividing all firing rates in the session by this value.

When analyzing binary behavioral outcomes of the experiment, such as the effect of ICMS parameters, visual condition, or timing offsets on whether the participant reported an ICMS-elicited percept, a logistic regression test was used to compute significance. The test was performed using the MATLAB function *mnrfit*, using nominal (softmax) regression.

Throughout the analyses, when multiple comparisons were performed, Bonferroni–Holm correction was performed to correct the *P* values.

Gaussian Curve Fitting

The percentages of trials where the participant reported simultaneous ICMS and visual percepts were fit to Gaussian curves (Fig. 4). Gaussians were fit to the raw percentages for each session and current amplitude reported in Fig. 4, *A* and *C*, using MATLAB's *fit* function, and restricted to peaks bounded by [0, 100] since the physical limits of simultaneous reports are 0% and 100%. A parametric bootstrap with 5,000 iterations was used to assess variance (25). In the bootstrap, a binomial distribution *B(n,p)* was fit to the raw data at every time point, in which n = the number of trials at that time point and p = the percentage of trials that were reported as simultaneous. On every iteration of the bootstrap, these binomial distributions were sampled using MATLAB's *binornd* function, and Gaussian curves were fit to the resulting synthetic data. 95% confidence intervals on the Gaussians and their peaks were computed by examining the distribution of Gaussians generated over the bootstrap. The point of subjective simultaneity was taken as the peak of the fitted Gaussians. The just-noticeable difference (JND) was taken as the time in milliseconds between the peak and the 25% point of the Gaussian curve.

A Gaussian model was chosen for its simplicity, given the relatively sparse sampling of temporal offsets in the data. A more complex model runs the risk of overfitting to the data and would require a larger number of time samples to better characterize the shape of the temporal binding window.

Modulation Analysis

The modulation of multiunit activity in each visual condition to the visual cue was assessed using the catch trials (*P1:* $n = 36$; *P2:* $n = 40$) collected during the realistic and abstract conditions, in which the visual cue was presented and the participant expected an ICMS-elicited sensation, but no ICMS was delivered. Significance of modulation of normalized neural responses was computed via linear regression analysis in 100-ms bins. A linear regression model attempted to explain neural firing rates as a linear combination of indicator variables (39). In this case, the indicator variables represented different time bins within the task relative to the visual animation. The model also accounted for resting firing rates, which were computed as the mean firing rates in the ITI, 1,750 ms to 750 ms before the onset of the "stimulation" phase (Fig. 1*B*). The resting neural firing rates and the firing rates from each time bin of interest in each trial, were fit to this equation:

$$F = \beta_0 + \beta_1 X_1 + \beta_2 X_2 + \ldots \beta_C X_C,$$

where F = vector of firing rates on each trial within each time bin and the average resting firing rate, X = one-hot-encoded matrix of time bin identity for each trial, β = estimated regression coefficients indicating level of modulation in each time bin, and C = number of time bins tested. F also

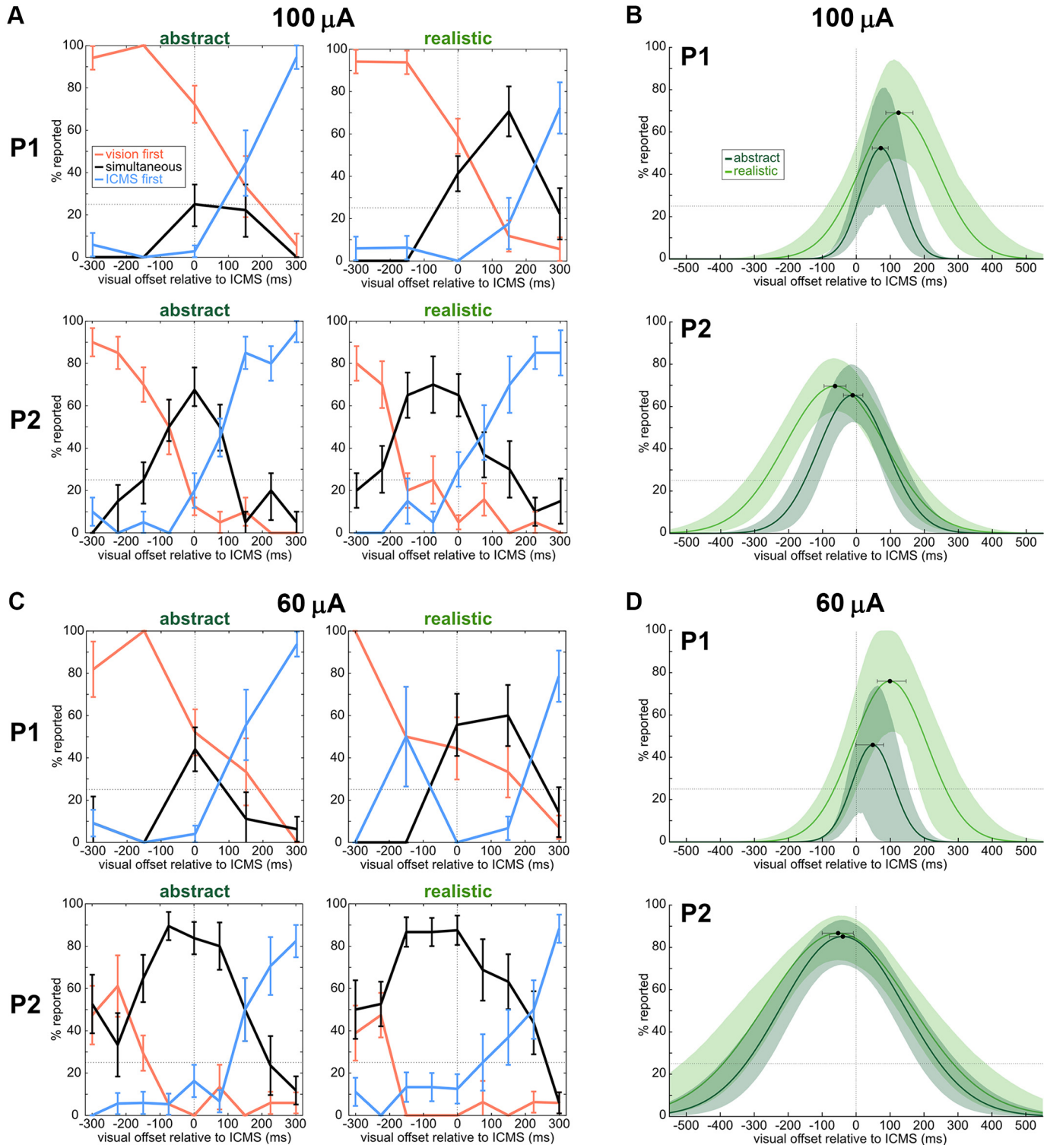

Figure 4. The temporal binding window between vision and intracortical microstimulation (ICMS). *A*: reports of stimulus order relative to the ground truth among 100 μA trials in each participant (*top row: P1*; *bottom row: P2*). A negative timing offset indicates the visual stimulus preceded ICMS. Horizontal dotted line indicates 25% mark. Error bars represent means ± SE. *B*: Gaussian curves fit to the "simultaneous" points (black lines) in (*A*) for each participant. Black dots indicate curve peaks. Shaded area and error bars on peaks represent 95% CIs generated through a parametric bootstrap fit to 5,000 synthetic versions of the data modeled with a binomial distribution (see METHODS). *C*: analysis identical to (*A*), in 60 μA trials. *D*: analysis identical to (*B*), in 60 μA trials.

included n additional entries corresponding to β_0 (n = the total number of catch trials), which contained the resting firing rate calculated as indicated earlier. Here, the regressors in β represent the expected change in firing rates from resting relative to the tested time bins, thus if a value in $\beta = 0$, then the model encodes no difference in firing rate between resting and the respective time bin. The null hypothesis $\beta = 0$ was assessed using a one-sample two-tailed Student's t test within each channel and time bin, and if the null hypothesis was rejected then the channel's firing rate was determined to be significantly modulated to the visual information compared with the resting firing rate. Within each channel, P values were corrected for multiple comparisons across time bins using the Bonferroni-Holm method.

To assess significant differences in the numbers of modulated channels across time bins and conditions, a bootstrap analysis was run for 1,000 iterations. In each iteration, the catch trials were randomly sampled with replacement and reassessed for significant modulation in each channel and time bin (Fig. 5*A*).

Representational Similarity Analysis and Multi-Dimensional Scaling

Normalized firing rate data, binned in 0.5 s phases, were examined using representational similarity analysis (RSA, Fig. 5*D*) (40, 41). The Python package *rsatoolbox* (Table 2, https://github.com/rsagroup/rsatoolbox) was used to compute representational dissimilarity matrices (RDMs). The measure of dissimilarity used was cross-validated Mahalanobis distance with multivariate noise normalization (42), in which the noise covariance matrix is estimated and regularized toward a diagonal matrix to ensure that it is invertible. The cross-validated Mahalanobis distance is an unbiased measure of square Mahalanobis distance, which also has a meaningful zero-point (42, 43). A distance of zero between two conditions indicates the underlying neural data is fully indiscriminable, and the larger the Mahalanobis distance, the more these neural patterns are discriminable.

Data were cross-validated in session-wise splits (*P1*: 9 sessions; *P2*: 10 sessions), each containing the four catch trials collected per run for each condition and divided into 0.5-s bins ("ITI," "Down," "Touch," "Up"). "ITI" was composed of the last 0.5 s of the ITI before the "Down" phase began. The RDM generated from this data is symmetric across the diagonal, with meaningless zeros on the diagonal itself (Fig. 5*D*).

To better visualize the relationships in the RDM, multidimensional scaling (MDS) was applied using the MATLAB toolbox *rsatoolbox* (Fig. 5*E*, Table 2, https://github.com/rsagroup/rsatoolbox_matlab) (41). MDS allows for distances in RDMs to be mapped to the 2-D plane as faithfully as possible, using a metric stress criterion to arrange points without any assumptions of category structure. The stress between points is visualized with gray lines between points, stretched like rubber bands—the thinner the band, the more the true distances between points should be closer together to be fully accurate to the original high dimensional RDM.

Eyetracking

Eye position [three-dimensional (3-D) coordinates] and gaze direction (3-D ray vector) within the VR environment were collected in both participants every 20 ms, giving six features to describe eye movements that were averaged into 50-ms bins to match the neural firing rate data. The headset software also returned a Boolean value indicating if the eye features were valid at each time point. If any time points within a 50-ms bin were marked as invalid, the entire time bin was marked invalid. Eye movements were analyzed within catch trials to match the neural data analysis described earlier. Trials were used if at least 60% of time bins were marked as valid. In *P1* (36 catch trials per condition), 12 realistic and 36 abstract trials were used. In *P2* (40 catch trials per condition), 26 realistic and 30 abstract trials were used.

Within the valid trials, eye movement features were each normalized within each run by calculating the mean resting value across the entire 2-s ITI period, and dividing all data in the session by this value (APPENDIX Fig. A2*B*). Significant modulation of eye features (APPENDIX Fig. A2*C*), RSA (APPENDIX Fig. A2*D*), and MDS (APPENDIX Fig. A2*E*) were then computed in the same manner as the neural data (see aforementioned), with the caveat that because the sets were missing trials, RSA was performed without cross-validation.

RESULTS

To understand the relationship between ICMS and visual context, behavioral and neural responses were recorded from two human tetraplegic patients (*P1*, *P2*), implanted with microelectrode arrays in S1 (Fig. 1*A*, Table 1) (Blackrock Neurotech, Salt Lake City, UT) as ICMS was delivered during a psychophysical task. Three conditions were collected and examined: the baseline, a realistic condition, and an abstract condition (Fig. 1, *B* and *C*).

During the baseline task, which was only tested in *P1*, ICMS was delivered without a visual stimulus (Fig. 1*B*). *P1* reported when a sensation was elicited, that sensation's anatomical location and intensity, and a one-word self-generated descriptor for the sensation's qualitative nature.

During the realistic and abstract conditions of the main task, both participants received ICMS while viewing a visual cue delivered either at a temporal offset or simultaneously (Fig. 1*C*, Supplemental Videos S1, S2, and S3). Participants reported on each trial if they felt a tactile sensation from ICMS, and in the affirmative case, if the visual cue was first, the ICMS-elicited sensation was first, or both cues were perceived simultaneously.

P1 also reported the same qualitative measures as during the baseline: ICMS sensation location, intensity, and a one-word descriptor. Due to constraints on data collection, *P2* only reported if a sensation was perceived, and the relative order of ICMS and the visual cue. Although *P2* did not report sensation location on each trial, he reported after each study session that the sensations were localized on the tip of his index finger.

This set of experiments was designed to assess the effect of visual context on ICMS percepts, with particular interest in how these two stimuli would be perceived in temporal relation to one another. Although similar to a classic two-alternative forced choice task, this paradigm allowed for participants to explicitly report when stimuli felt simultaneous to better characterize the perceptual experience of ICMS. In

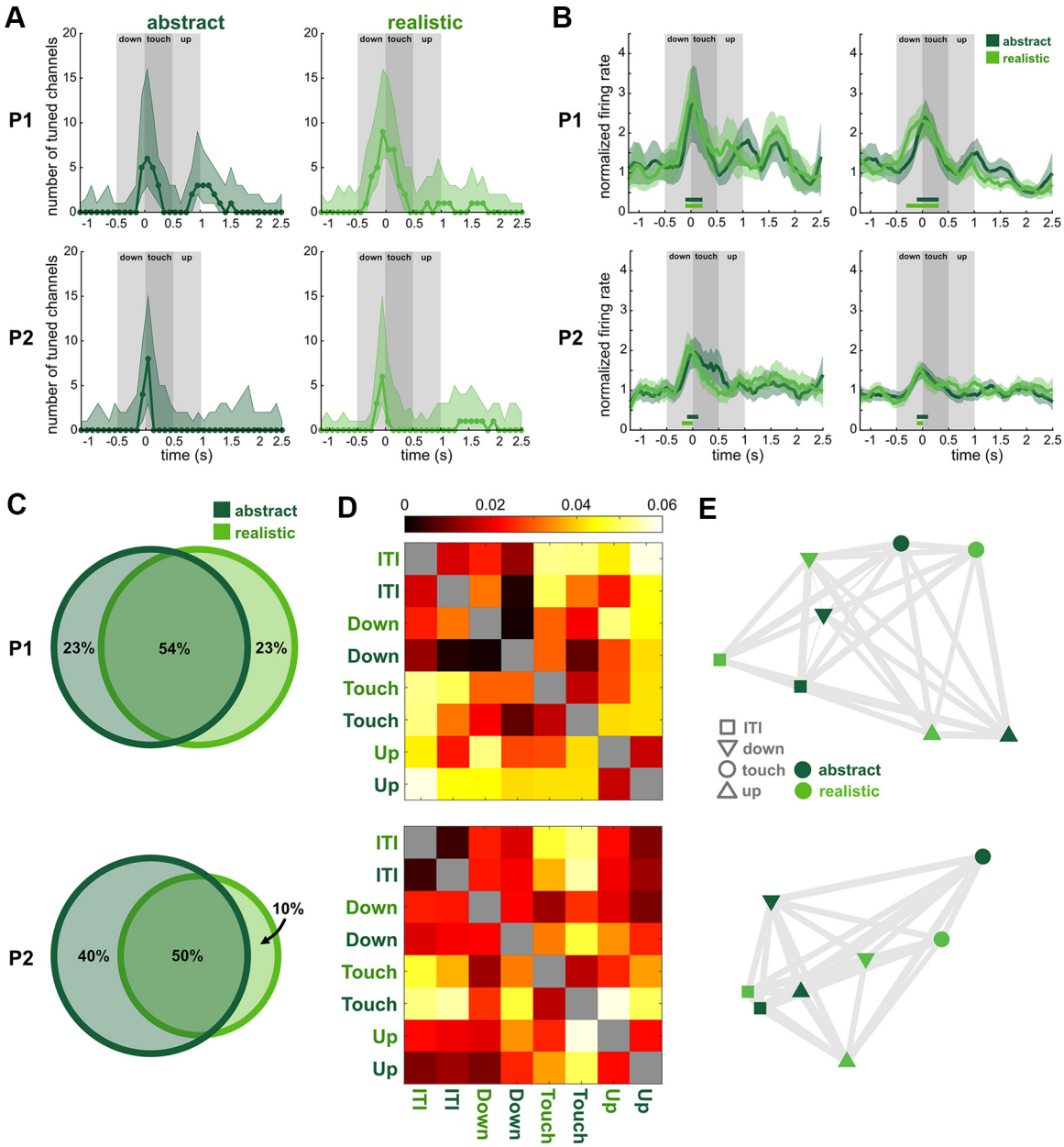

Figure 5. Neural activity during catch trials. *A*: number of channels significantly modulated during catch trials relative to resting (*P1* $n = 96$ channels, *P2* $n = 128$), separated by condition. Time is aligned to the onset of the "touch" phase of the visual stimulus. Shaded area indicates 95% confidence intervals (CIs) computed by bootstrapping across trials (*P1* $n = 36$ trials, *P2* $n = 40$) over 1,000 iterations. Significant modulation was assessed by linear regression analysis (see METHODS). *B*: example modulated channels with firing rates averaged across catch trials, by condition. For visualization only, firing rates were smoothed using a first-order Savitzky-Golay filter. Horizontal bars indicate the times in which the firing rates of the channels were significantly modulated relative to resting firing rates, color-coded by condition. Shaded area corresponds to SE. *C*: Venn diagrams depicting the overlap in channels with significant modulation in abstract and realistic conditions. Percentages are based on the total number of channels with significant modulation at any point during the visual animation (*P1*: 13 channels, *P2*: 10 channels). *D*: representational dissimilarity matrices (RDM) of multiunit neural activity across all channels. Heatmap indicates distances between neural activity patterns associated with each condition and task phase [e.g. realistic intertrial interval (ITI) in *top left*], which are computed as the cross-validated Mahalanobis distance with multivariate noise correction; a distance of 0 indicates conditions are statistically indistinguishable. Each phase represents 0.5 s of averaged firing rates; the ITI is based on the 0.5 s immediately prior to "down" phase of visual stimulus. Analysis was not run on the diagonal (gray boxes). *E*: multidimensional scaling (MDS) plots of the RDMs in (*D*). Axes are arbitrary. Gray lines between icons are "rubber bands" whose thickness is based on the goodness of fit of the scaling (*P1*: Pearson's $r = 0.93$, $P = 1.5 \times 10^{-12}$; *P2:* $r = 0.97$, $P = 4.9 \times 10^{-17}$). Thinner, more "stretched" bands indicate that the icons are closer together in the original high-dimensional space than they are shown to be.

addition, catch trials without ICMS made it possible to examine the neural response of S1 to visual information.

Behavioral accuracy was computed by comparing the participants' assessments of relative ICMS and visual stimulus order with the ground truth (the times at which the stimuli were actually presented). There was no learning effect: accuracy did not meaningfully change over the different session days (Fig. 1*D*, *F*-test vs. constant model, *P1:* $P = 0.58$; *P2:* $P = 0.14$). For *P1*, behavioral performance was unaffected by the visual condition (Fig. 1*D*, logistic regression test $P = 0.15$),

whereas *P2*'s performance was slightly better ($P = 0.027$) in the abstract condition (mean = 60.5%, std = 6.3%) than in the realistic condition (mean = 52.8%, std = 8.4%).

ICMS-Elicited Tactile Sensations

On each trial, the participants reported whether or not they sensed a tactile percept. Three different ICMS current amplitudes were tested (100, 60, 30 μA), and catch trials were also collected where no ICMS was delivered. *P1* never reported a sensation in a catch trial. *P2* reported one sensation during a catch trial; all data collected on that day was discarded and was not used for further analyses. There was a strong effect of ICMS current amplitude on the probability of *P1* reporting a percept on a trial in the baseline trials (logistic regression test, $P = 1.7 \times 10^{-9}$) as well as on the probability of both participants reporting a percept in both visual conditions of the main task (logistic regression test, *P1:* $P = 3.2 \times 10^{-33}$; *P2:* $P = 1.9 \times 10^{-71}$; Fig. 2). In both participants across conditions, at 100 μA current amplitude, sensation detection was essentially at ceiling (*P1* baseline mean: 100%, 95% confidence interval (CI) = [100, 100], abstract: 98.1% [95.4, 100], realistic: 94.4% [89.8, 98.1]; *P2* abstract: 100% [100, 100], realistic: 99.5% [98.5, 100]). At 30 μA, sensation detection was near floor (*P1* baseline: 4.4% [0, 11.1], abstract: 1.9% [0, 4.6], realistic: 2.8% [0, 6.5]; *P2* abstract: 19.5% [14.5, 25], realistic: 15.5% [11.0, 20.5]).

In contrast, during 60 μA ICMS trials, the baseline elicited more felt sensations than the visual conditions in *P1* (Fig. 2*A*, logistic regression test, $P = 3 \times 10^{-4}$; *P1*: baseline mean = 95.6%, 95% CI = [88.9, 100]; abstract mean = 63.9%, [54.6, 72.2]; realistic mean = 55.1%, [44.9, 65.0]).This effect may be due to the fact that in the baseline, *P1*'s only task was to report if he felt a sensation and its qualitative affect. In the other conditions, *P1* was also tasked with attending to visual stimuli and reporting the relative temporal order between visual and ICMS percepts. Since the baseline task represented a lower cognitive load than the other conditions, it may have been easier to detect near-threshold ICMS percepts.

However, in both *P1* and *P2* (*P2* 60 μA trials: abstract mean = 88.5%, [84, 92.5]; realistic mean = 84.3%, [79.3, 89.4]) the probability of a trial yielding a sensation was not different between realistic and abstract conditions (logistic regression test, *P1:* $P = 0.12$, *P2:* $P = 0.19$).

Within the realistic and abstract conditions, the probability of *P1* reporting a sensation was significantly affected by the timing offset between visual and ICMS cues (logistic regression test, $P = 5.5 \times 10^{-4}$), but this relationship was not significant for *P2* ($P = 0.19$) (APPENDIX Fig. A1). Thus, the effect of stimulus timing on the probability of sensations felt was inconclusive. When *P1* reported a sensation, he also reported the intensity of the sensation using a subjective number scale (Fig. 3*A*), the sensation location (Fig. 3*B*), and a single word descriptor about how the sensation felt (Fig. 3*C*). Across baseline, realistic, and abstract trials, there was no effect of trial condition on intensity ratings, but there was an effect of current amplitude (two-way ANOVA, condition: $P = 0.82$, current: $P = 8.2 \times 10^{-23}$, condition-timing interaction: $P = 0.78$). Similarly, within just realistic and abstract trials, there was no effect of condition or stimulus timing on intensity ratings, but there was an effect of ICMS current amplitude (three-way ANOVA, condition: $P = 0.69$, timing: $P = 0.49$, current: $P = 1.5 \times 10^{-17}$, all interaction effects $P > 0.05$). Comparing 100 μA and 60 μA specifically, the greater amplitude led to greater intensity ratings (unpaired two-tailed *t* test, $P = 1.2 \times 10^{-21}$).

The location of individual ICMS-elicited sensations reported by *P1* never exceeded the bounds of one box (~5 cm × 5 cm) in the grid provided as a reference during data collection. Reported locations were highly similar across conditions and current amplitudes, with the bulk of reported sensations being localized to the posterior forearm (Fig. 3*B*).

Across nine sessions, the majority of sensations reported in all conditions were cutaneous; proprioceptive sensations (e.g., "move right") occurred infrequently during baseline trials and never during the visual conditions (Fig. 3*C*). Within 100 μA trials, the word "touch" was used to describe the sensation in both realistic and abstract trials a higher proportion of the time than in the baseline (Fig. 3*C*, 100 μA trials, Wilcoxon signed-rank test, realistic $P = 0.02$, abstract $P = 0.03$). In addition, within 100 μA trials, "touch" was used more frequently in realistic trials than in abstract trials ($P = 0.03$) Similarly, in 60 μA trials, the highest proportion of "touch" sensations occurred in the realistic condition and the lowest occurred in the baseline, but this trend was not significant (Fig. 3*C*, 60 μA trials realistic vs. baseline: $P = 0.41$, abstract vs. baseline: $P = 0.5$), nor was the difference between the amount of "touch" percepts in realistic trials compared to abstract trials ($P = 0.5$). Across all conditions, the word "touch" was used more in 60 μA trials than 100 μA trials ($P = 0.004$).

The Temporal Binding Window between Vision and ICMS

In every trial of the realistic and abstract conditions that the participants reported an ICMS-elicited sensation, they reported the perceived order of the ICMS and visual cue. Specifically, participants could either state that one stimulus came before the other or that they occurred simultaneously (Fig. 4, *A* and *C*). Overall, the likelihood of *P1* giving a "simultaneous" answer was affected both by timing offset (logistic regression test, $P = 0.01$) and visual condition ($P = 0.001$), but not current amplitude ($P = 0.27$). The likelihood of *P2* giving a simultaneous answer was affected by timing offset ($P = 4.2 \times 10^{-5}$), visual condition ($P = 0.04$), and current amplitude ($P = 7.7 \times 10^{-15}$).

To further examine how visual condition affected perceived timing, participant responses were examined within the two current amplitudes tested with the largest number of perceived sensations: 100 μA and 60 μA (Fig. 2). Unsurprisingly, in both conditions and at both current amplitudes, the participants detected the correct order most easily in the −300 and 300 ms offset trials (Fig. 4, *A* and *C*). In *P1*, within each ICMS current amplitude, the areas under the "simultaneous" curves were different between realistic and abstract conditions (100 μA: $P = 3 \times 10^{-4}$; 60 μA: $P = 0.005$). In *P2*, the areas were only different within 100 μA trials (100 μA: $P = 0.04$; 60 μA: $P = 0.11$).

To better quantify when stimuli were perceived as occurring simultaneously within 100 μA trials, the "simultaneous" curves (Fig. 4, *A* and *C*, black lines) were fit to Gaussians which allowed for interpolation between the tested timing offsets (Fig. 4, *B* and *D*). The variability in the data was assessed using a parametric bootstrap (see METHODS) (25). The point of subjective simultaneity (PSS), defined as the

peak of the fitted Gaussians, occurred when ICMS preceded the visual cue for both visual conditions in *P1* (abstract: 72.2 ms, 95% CI = [47.0, 94.2]; realistic: 124.2 ms [86.8, 166.8]). In *P2*, the opposite was true: the PSS occurred when the visual cue preceded ICMS (abstract: −11.4 ms, 95% CI = [−38.7, 18.6]; realistic: −63.2 ms [−95.9, −30.7]).

The just-noticeable difference (JND), defined as the time in milliseconds between the peak and the 25% point of the Gaussians, was larger in realistic trials (*P1*: 164.0 ms [113.6, 221.8]; *P2*: 209.6 ms [167.7, 247.4]) than in abstract trials (*P1*: 72.3 ms [24.0, 95.6]; *P2*: 141.7 ms [105.1, 169.8]), although this difference was only significant in *P1*. In *P1*, the 25% point on the left side of the Gaussian was not different between realistic and abstract conditions, whereas the 25% point on the right side was different across conditions: the realistic condition had a larger offset than the abstract condition. In *P2*, the reverse was true: the 25% point on the left side was larger in the realistic condition than in the abstract condition, whereas the right-hand 25% point was not different across conditions.

The data within 60 μA trials were also fit to Gaussians using the same procedure (Fig. 4*D*). In *P1*, the 60 μA realistic PSS (98.8 ms [61.3, 146.5]) was not significantly different from the abstract PSS (48.3 ms [−1.1, 80.4]). The 25% points of the Gaussians were also not different from one another between the realistic condition and the abstract condition. However, in *P1* the JND was larger in the realistic condition (164.0 ms [98.1, 217.2]) than in the abstract condition (66.6 ms [0.1, 95.7]). In *P2*, the realistic PSS (−53.0 ms [−100.0, −8.2]) was not significantly different from the abstract PSS (−39.1 ms [−78.4, −5.9]). The JNDs were also similar across conditions in *P2* (realistic: 338.7 ms [281.3, 430.6]; abstract: 286.1 ms [230.4, 339.1]). Neither the left nor the right 25% point of the Gaussian was different across conditions.

S1 Neural Responses to Visual Stimuli

In both participants, neural activity was recorded in the S1 microelectrode arrays during catch trials, when no ICMS was delivered. Multiunit channel firing rates were computed, and the modulation of channels relative to resting (during the ITI) while visual stimuli were delivered was assessed using a linear regression analysis (Fig. 5, *A* and *B*). In both *P1* and *P2*, the highest number of modulated channels in the realistic condition was in the −0.1 s to 0 s bin prior to visual touch, during the end of the "motion down" phase. With respect to the abstract condition, the peak number of modulated channels occurred in the bin immediately after "visual touch" phase onset, 0 to 0.1 s in both participants. The timecourse of two example modulated channels from each participant are shown in Fig. 5*B* (see APPENDIX Fig. A2*A* for channel rasters and peristimulus time histograms).

In *P1*, 10 channels exhibited significant modulation during the realistic visual animation and 10 exhibited significant modulation during the abstract visual animation. In *P2*, six channels exhibited significant modulation during the realistic visual animation and nine exhibited significant modulation during the abstract visual animation. This measure was calculated by counting the number of unique channels with significantly modulated firing rates in any of the 100-ms bins during the entire visual animation, including down, touch, and up (total animation length: 1.5 s). The overlap in channels with significant modulation in the realistic and abstract conditions during the visual animation (1.5 s total) was quantified (Fig. 5*C*). In both participants, more channels were significantly modulated in both realistic and abstract conditions, than were significantly modulated in either condition exclusively.

To understand the population response in S1 to the visual stimuli, representational similarity analysis (RSA) was employed on the firing rates of all channels in each participant (Fig. 5*D*) (40), using cross-validated Mahalanobis distance with multivariate noise correction (42). Multidimensional scaling (MDS) was used to visualize the computed distances between condition phases (Fig. 5*E*) (41). In *P1*, the data were grouped more tightly by task phase (ITI, down, touch, up) than by condition (abstract, realistic), as assessed by a Wilcoxon rank sum test on distances within phases/across conditions versus distances within conditions/across phases ($P = 0.03$). Qualitatively, this is apparent in the MDS where icons are grouped by phase, but the conditions are intermixed together (Fig. 5*E*), which indicates that the neural activity was similar between the two visual conditions, and varied along the timecourse of the task in both conditions. In *P2*, a similar grouping is visually present to some extent (Fig. 5*E*), but the distances within phases/across conditions were not significantly different compared with the distances within conditions/across phases ($P = 0.13$).

It is possible that eye movements confounded the neural data, given the importance of visual information during this task. To assess this possibility, catch trials with valid eye tracking data were analyzed using the same linear regression analysis as the neural data (APPENDIX Fig. A2*C*; *P1*: 36 abstract trials, 12 realistic; *P2*: 30 abstract, 27 realistic). None of the six eye movement features were modulated relative to resting during the vast majority of the visual animation in both participants, and the earliest that firing rate modulation occurred was immediately after the visual animation in *P1*, and during the final 0.25 s of the 1.5 s animation in *P2* (APPENDIX Fig. A2, *B* and *C*). The eye movement features were also used to perform RSA using Mahalanobis distance with multivariate noise correction (APPENDIX Fig. A2*D*), and mapped to two dimensions using MDS (APPENDIX Fig. A2*E*). Eye movements were highly clustered according to visual condition compared with task phase (Wilcoxon rank sum test on distances within phases/across conditions vs. distances within conditions/across phases, *P1:* $P = 0.001$; *P2:* $P = 0.001$) as is visually apparent in the MDS plots.

DISCUSSION

Behavioral and neural data from two tetraplegic participants (*P1*, *P2*) receiving ICMS in S1 (Fig. 1*A*) while observing visual abstract or realistic touch cues (Fig. 1*C*, Supplemental Videos S1, S2, and S3) were examined. Visual cues were delivered at varying temporal offsets relative to ICMS (Fig. 1*B*) and the participants reported the perceived order of these cues. *P1* also reported descriptive information about the ICMS-elicited tactile sensations. This experiment yielded three main findings: *1*) the qualitative percepts of ICMS-elicited sensations are influenced by visual information and ICMS current amplitude; *2*) the temporal binding window between ICMS and vision varies based on the biological

relevance of the visual stimuli; *3*) S1 represents visual information relevant to ICMS in a context-independent fashion.

ICMS-Elicited Sensations Are Affected by Visual Information and ICMS Current Amplitude

This work replicates the previously known result that higher ICMS current amplitudes tend to elicit sensations more frequently (Fig. 2), and the sensations tend to be of higher intensity (Fig. 3*A*) (12, 13, 19). However, we also find an interaction between current amplitude and vision. During 60 μA trials, the percentage of trials that elicited a sensation through ICMS were significantly higher in the baseline than in either of the visual conditions (Fig. 2*A*). Since 60 μA ICMS is typically perceived to be lower intensity than 100 μA ICMS (Fig. 3*A*), it is closer to the perceptual detection threshold. The added cognitive load of attending to a visual stimulus while simultaneously attending to ICMS may be responsible for lower rates of reported sensations. Indeed, this behavioral result is predicted by the divisive normalization model of attention, which suggests that when neurons respond strongly to attended stimuli, neural responses to other stimuli are proportionally suppressed (44, 45).

We also demonstrate an interaction effect of ICMS current and visual condition on the qualia of sensations elicited in *P1*: "touch" was used as a descriptor more often at 60 μA than at 100 μA, and within 100 μA the word "touch" was used more often in the realistic condition than in the baseline or the abstract condition (Fig. 3*C*). The increased use of the word "touch" in lower current amplitude trials may be because within the participant's subjective framework, the word "touch" could represent a tactile stimulus that is inherently of a lower intensity than other descriptors like "squeeze" or "grab." Of the words the participant used to describe sensations, which were freely chosen by him, "touch" appears to be the one that most closely matches the visual touch depicted in the realistic condition. We additionally note that proprioceptive qualia were only reported during the baseline, and never reported during visual trials, perhaps indicating a visually-mediated bias toward cutaneous percepts and away from proprioceptive percepts in this experiment. We note that the "realistic" scene was visually complex, so further work will be necessary to establish whether the effects we report here are emergent from realistic scenes depicting visual touches as a whole, or if the effects were triggered by specific aspects of this visual condition.

Although previous work has shown that visual information can bias the perceived location of peripheral intraneural stimulation (28), the effect reported here suggests that visual information can also bias the qualitative percept of ICMS-elicited sensations. When ICMS is employed on the same electrode, with the same parameters, in the same participant, widely varying qualia often result (Fig. 3*C*, baseline charts) (12, 13). A viable neural prosthetic would ideally be able to elicit naturalistic sensations of specific qualia as needed (46). If visual information can stabilize ICMS percepts to some extent, this has the potential to be highly important to the development of such a tactile neural prosthetic.

The Biological Relevance of Visual Stimuli Influences the Temporal Binding Window

Visual stimuli were presented at varying temporal offsets (0–300 ms) relative to ICMS (Fig. 4). In *P1*, the PSS occurred when ICMS preceded the visual cue, with a lag of ∼50–125 ms depending on visual condition and ICMS current amplitude (Fig. 4, *B* and *D*). In *P2*, the PSS occurred when the visual cue preceded ICMS, with a lag of ∼10–65 ms. The variance in the PSS of the two participants may be due to individual differences, differences between the properties of stimulating electrodes, or differences in microelectrode implant location—or some combination of these factors. We do not conclude that there is some constant temporal offset between ICMS and vision, but rather that future ICMS applications should not assume that the temporal binding window is centered at zero. This finding echoes prior work with amputees, which has shown that the PSS of peripheral nerve stimulation shifts depending on whether the upper or lower limb is stimulated (27). Although the stimulation delivered in this work is intracortical rather than peripheral, and both participant's microelectrode arrays were implanted in putative S1, *P1*'s array is located in the arm region (47) and *P2*'s array is located in the finger region (see METHODS); this difference in cortical subregions may be sufficient to create processing time differences.

Aside from anatomical considerations, the sensory processing systems of different individuals are often equipped with different priors about the environment, biasing them toward one perceptual experience or another. A striking example of this phenomenon in the visual system is the viral photo of a dress that is perceived as either blue-black or white-gold due to varying assumptions by the visual system about the photo's illumination (48). It is possible that *P1* and *P2* have different biases with respect to how they process visuo-tactile information.

Finally, stimulation occurred on a single electrode in each participant, chosen due to its reliability in eliciting tactile percepts in prior experiments. It is highly possible that multi-channel stimulation would give rise to a different PSS than single-channel stimulation, even within a single participant, given that reaction times to ICMS are shorter with multi-channel stimulation than single-channel stimulation (18). Although outside of the scope of this work, our findings highlight the need to determine how the PSS changes across ICMS stimulation parameters and brain areas, and in individual patients. Regardless of the direction of the offset, the existence of a perceptual lag between vision and ICMS in both participants indicates that the parameters used here, which are standard in the field, do not allow ICMS to be perfectly integrated into a temporally well-aligned multisensory experience.

Another indicator that ICMS and vision are not perfectly integrated is the ceiling effect observed in both participants: the maximum percentage of trials within each timing offset, visual condition, and ICMS amplitude that was perceived as simultaneous was 70.6% (SE = 58.8%, 82.4%) in *P1* and 85.0% (78.3%, 91.7%) in *P2*. It is possible that the time points sampled were not fine enough to pick up the true PSS of each participant, but the peak of the fitted Gaussians also suggests that there is no time point at which ICMS would feel simultaneous with a visual stimulus 100% of the time. Further research is necessary to determine whether this effect is an inherent limitation of ICMS or due to participant expectations of temporal offsets being present in this specific task.

Although the PSS remained relatively consistent within each participant across visual conditions, the width of the

temporal binding window varied between visual conditions. In both participants, during 100 μA trials, both the area under the curve of "simultaneous" answers (Fig. 4*A*) and the JND (Fig. 4*B*) were larger in realistic trials compared with abstract trials, indicating the temporal binding window between ICMS and vision is larger in the realistic condition. In other words, the participant was more likely to perceive ICMS and vision as occurring simultaneously in the realistic condition, and more likely to assign an order to the stimuli in the abstract condition.

In 60 μA trials, the area under the curve and the JND were larger in realistic trials for P1, just as in 100 μA trials (Fig. 4, *C* and *D*). In *P2*, the fitted Gaussian realistic curve was larger than the abstract one, and the realistic JND was larger than the abstract JND, although these differences were not significant. Since 60 μA ICMS is less perceptible than 100 μA ICMS (Fig. 2) (12, 13, 19), *P2* may have integrated this weaker signal more easily with the visual cue across visual conditions, resulting in more "simultaneous" answers overall. Supporting this theory, we report an effect of current amplitude in the rate of "simultaneous" answers for *P2*, but no such effect for *P1*.

As a whole, the temporal binding window results indicate that a biologically relevant touch input allows the brain to more easily link visual and ICMS inputs together causally, and view them as happening as part of the same event, whereas in an abstract context, visual and ICMS inputs are more likely to be interpreted as two separate events. Since a somatosensory neural prosthetic using ICMS would be deployed in a real-world environment, this result is encouraging because it supports the idea that the brain is able to combine multisensory realistic inputs with artificial stimulation to generate visually plausible sensations (28). Further work is necessary to determine whether visual and ICMS cues are combined in a statistically optimal way to determine causality, as has been shown in the visuo-haptic literature on Bayesian causal inference (49, 50).

It is possible that changes to the temporal binding window could be due to differences in task difficulty across the visual conditions. The abstract condition is a comparatively simple visual stimulus (Fig. 1*C*, Supplemental Video S1), centered in the visual field, so it may be easier to estimate timings in this condition than in the more complex realistic condition (Fig. 1*C*, Supplemental Videos S2 and S3). Yet, the visual conditions were relatively well-matched in terms of difficulty: *P1* performed equally well at assessing stimulus order between visual conditions, and although *P2* performed slightly better at the abstract version of the task, the accuracy histograms of the two conditions were highly overlapping for both participants (Fig. 1*D*). In addition, the ability of the participants to gauge the timing between ICMS and visual cues was not affected by learning, as across the experimental sessions (*P1:* $n = 9$; *P2:* $n = 10$) there was no change in the participants' ability to accurately assess stimulus order. It is therefore unlikely that learning over time or task difficulty were major confounds in these findings.

S1 Represents ICMS-Relevant Visual Content in a Context-Independent Fashion

Examining catch trials during which visual stimuli were presented without ICMS, we find that a significant number of channels have significantly modulated firing rates in response to visual touches relative to resting activity (during the ITI) in both participants (Fig. 5*A*). In particular, S1 activity has the most modulated channels during the initial onset of the visual touch. Given that a total of 13 S1 channels in *P1* and 10 S1 channels in *P2* have modulated firing rates during the visual animations, it is clear that S1 reflects some component of the visual stimulus even when there is no ICMS or physical tactile event. Although abstract trials elicited modulated activity peaking during the first 100 ms of the visual touch onset, modulated neural activity during realistic trials peaked 100 ms before the onset of visual touch, during the "motion down" period, indicating possible preparatory or predictive activity (51).

There was substantial overlap between the channels whose firing rates were modulated by abstract and realistic trials in S1. Many of the channels that were modulated by the realistic condition were also modulated by the abstract condition (Fig. 5, *B* and *C*). In a population-level analysis, RSA demonstrated that neural activity was not grouped by visual condition, as might be expected if the S1 response to realistic visual touches was drastically different from abstract visual touches, but instead neural activity was grouped by task phase (Fig. 5*D*). This grouping was significant in *P1*, but not for *P2*, although it was qualitatively present in the MDS for both participants (Fig. 5*E*). As discussed earlier, a possible reason for the variance between participants is that the locations of the microelectrode arrays are in different topographic regions of S1 (*P1*: arm area; *P2*: finger area), and may be positioned slightly differently within the tactile processing hierarchy (Fig. 1*A*).

Taken as a whole, these results indicate that S1 represents information contained in visual stimuli, and that this information generalizes across abstract and realistic conditions to some degree. Given that abstract and realistic stimuli are very visually distinct (Fig. 1*C*, Supplemental Videos S1, S2, and S3), it is unlikely that S1 is representing the actual visual inputs themselves. In the lateral intraparietal area, a region that responds to passive visual stimuli and to saccade planning and execution, there is prior work demonstrating that the multisensory requirements of a task can cause a neural population to become tuned to auditory information in addition to visual information (52), and that these tuned responses are supramodal, linking oculomotor behavior to selected auditory targets (53). Similarly, in the experiments presented here, S1 represents some aspect of the visual information that is relevant to the tactile aspect of the task and which generalizes across the two visual contexts in order to differentiate resting and visual touch activity.

Eye movements represent a potential confound for these results—S1 could simply be reflecting changes in eye movement pattern during the different task phases. To control for this possibility, eye movements were recorded in both participants in catch trials, and no eye movement features were significantly modulated relative to resting during the first 1 s of the visual animation ("down" and "touch" phases, APPENDIX Fig. A2, *B* and *C*), in either visual condition. Unlike the neural data, eye movements were also overwhelmingly clustered according to visual condition in an RDM analysis (APPENDIX Fig. A2, *D* and *E*). It is therefore highly unlikely that eye movements contribute to the neural patterns discussed here.

Prior work examining the interaction between real physical touches and vision with one of the participants in this study (*P1*) showed that S1 did not respond to visually depicted

touches without a physical tactile stimulus accompanying them (47). In contrast, the results from *P1* and *P2* in this study show that S1 does reflect information in visual stimuli without ICMS or other tactile stimuli. This difference in results supports a hypothesis suggesting that task design has a large effect on whether S1 represents visual information related to touch (47, 54). Rosenthal et al. (47) used a passive design, in which the participant merely observed tactile stimuli, whereas this study implemented a more active task in which the participant was required to describe perceived tactile sensations and report the order of ICMS and visual stimuli. This effect of task design on S1 modulation by visual stimuli can also be seen in the neuroimaging literature. Experiments with an active task tend to find that S1 responds to observed touches (55–61), whereas experiments with a passive task, or a task that is not touch-related, tend to find the opposite (31, 32, 62). Visual information not related to tactile stimulation also does not modulate somatosensory cortex (63). This effect of passive versus active tasks has a parallel in nonhuman primates. The lateral intraparietal area typically responds to passive visual stimuli but not passive auditory stimuli. After training on a saccade task with auditory cues, neurons become responsive to auditory stimuli that represent saccade targets (52). It is therefore likely that sensory processing, from early cortical stages like S1 to posterior parietal cortex, can flexibly incorporate multisensory information in a context-dependent way, based on higher-order feedback from brain areas responsible for multisensory integration.

Given that S1 can reflect visual stimuli based on task relevance, it is likely that biological relevance plays some role in what S1 represents in a given context (54, 64, 65). Modulation based on biological relevance may also underlie the visual enhancement of touch, a phenomenon in which tactile perception is improved when the body part being touched is visible, even if the visual input is noninformative about the touch (66–70). It may also play a role in S1's ability to reflect top-down concepts like affective significance, motor planning, and imagined touches (71–74).

However, it also seems apparent that when S1 represents information from vision, this encoding is temporally closely locked to the visual touch itself. In this work, we see that the onset of channel firing rate modulation never occurs more than 200 ms ahead of visual touch onset, and the majority of responses occur with 100 ms of visual touch onset, despite the visual animation starting 500 ms before visual touch onset (Fig. 5*A*). In prior work with participant *P1*, visual information predictive of when a physical touch would occur did not activate S1 ahead of the physical touch (47), and while the execution of a motor imagery task activates S1, visual cues relating to motor imagery are not sufficient to meaningfully activate S1 in the 4 s before performing the imagery (75). Therefore, while visual information is capable of modulating S1 (47), there is a limited predictive effect of visual information in S1. These results are indicative of higher-order efference copy signals that are computed outside of S1 as components of a forward model, perhaps to be used for predicting the sensory consequences of a movement. Similarly, the visual response documented here is likely implemented by higher order brain areas that represent the task requirements and compute a relevance threshold for different sensory inputs, which can then be implemented in modality-specific early processing areas such as S1. However, our results are not sufficient to untangle exactly what factors are driving visually evoked neural activity in S1, which could potentially be due to attention, expectation, tactile mental imagery, multisensory integration, or a combination of any of these factors.

Finally, the fact that our results are consistent with other characterizations of S1 in tactile studies indicates that S1 processes visual stimuli related to ICMS in some similar ways to visual stimuli related to real physical touches. This suggests that ICMS can be a valid substitute for physical touches in tactile tasks, not only in terms of behavioral performance (33, 46, 76), but also in terms of how the stimulation is processed within the somatosensory system.

Conclusion

To understand the behavioral and neural relationship between ICMS and vision, we examined responses to paired visual and ICMS stimuli at varying temporal offsets in a case study of two tetraplegic patients. This data set yielded two behavioral findings. The first is that the interpretation of ICMS-elicited sensations is affected by ICMS current amplitude, and by visual content. The second is that the temporal binding window between ICMS and vision varies in offset but is not necessarily centered at zero, and that the size of the temporal binding window is affected by the biological relevance of the visual stimulus. Studies of ICMS frequently examine elicited sensations without including any other type of sensory context (12, 13, 19, 77). Although these studies represent important foundational work, it will be important for a real-world BMI to fully understand how ICMS interacts with a richly complex sensory environment to stabilize touch percepts and create temporally aligned, unified multisensory experiences.

By examining the neural encoding of catch trials in which visual touches were present without ICMS, this work also adds to our understanding of how S1 represents visual information related to tactile sensations. We find that in an active task, S1 firing rates change during a visual touch relative to resting, in a relatively constant way across visual contexts. This finding supports the idea that high-level task-related variables in visual stimuli are represented in S1 and modulated by higher-order cognitive brain areas based on attention.

Further experiments should aim to investigate these findings across a larger set of ICMS parameters and electrodes, to better understand how the temporal binding window can vary based on stimulation properties. In addition, it will be important to explore in more depth how ICMS is integrated with other sensory systems and with varying levels of realism, as well as how S1 processes these inputs. By understanding multisensory ICMS integration both behaviorally and neurally, we can better use ICMS to design stable, naturalistic artificial tactile sensations.

Limitations of the Study

Although this case study expands our understanding of how vision is integrated with ICMS, it is limited in scope. Only two visual conditions (realistic and abstract) were tested; it would be necessary to test additional levels of visual realism to fully understand which components of the realistic scene contribute most to the results presented here. Testing two participants allows for an initial understanding

of how individual differences contribute to our results, but further work will be necessary to fully characterize the possible variance across patients. Furthermore, each participant received ICMS from only one electrode location, with a limited set of ICMS parameters, and it is likely that the qualitative nature of ICMS and the precise temporal relationship between ICMS and vision will shift if slightly different brain regions or parameters are tested. Finally, it is possible that demand characteristics of the task influenced *P1*'s description of sensation qualia, although we note that *P1* never reported a sensation in a catch trial, and reported significantly fewer sensations at lower current amplitudes, despite never being informed of the current amplitude being delivered on any given trial.

APPENDIX

Here, we provide more detailed analyses of behavioral and neural data. In APPENDIX Figure A1, we plot the rate at which participants reported tactile sensations, based on the amplitude of ICMS delivered and the timing offsets of this stimulation relative to visual cues. In APPENDIX Figure A2, we provide raster and peristimulus time histograms for example S1 channels during catch trials in both participants (APPENDIX Fig. A2*A*). We also plot the eye position and gaze direction for each participant across trials (APPENDIX Fig. A2*B*), and perform RSA on these eye features to construct MDS plots (APPENDIX Fig. A2*C*, *D*, *E*) in order to map the relationship of eye movements to the visual cues presented.

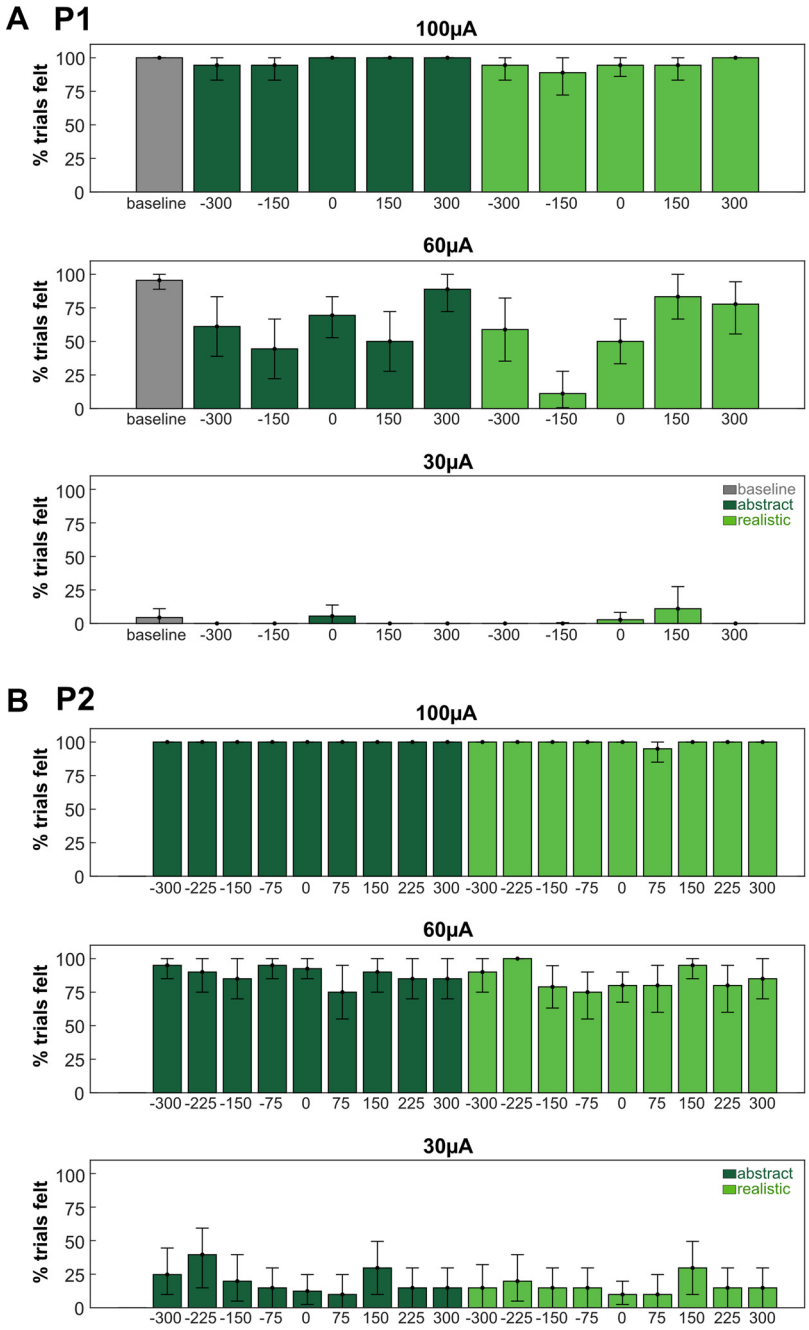

Figure A1. Tactile sensation rates within timing offsets and intracortical microstimulation (ICMS) amplitudes. *A*: percentage of trials eliciting a sensation across conditions in participant *P1*, sorted by ICMS current and timing offset. Error bars represent 95% confidence intervals (CIs) assessed by bootstrapping values across 1,000 iterations sampling from trials with replacement. *B*: analysis identical to (*A*), using data from participant *P2*.

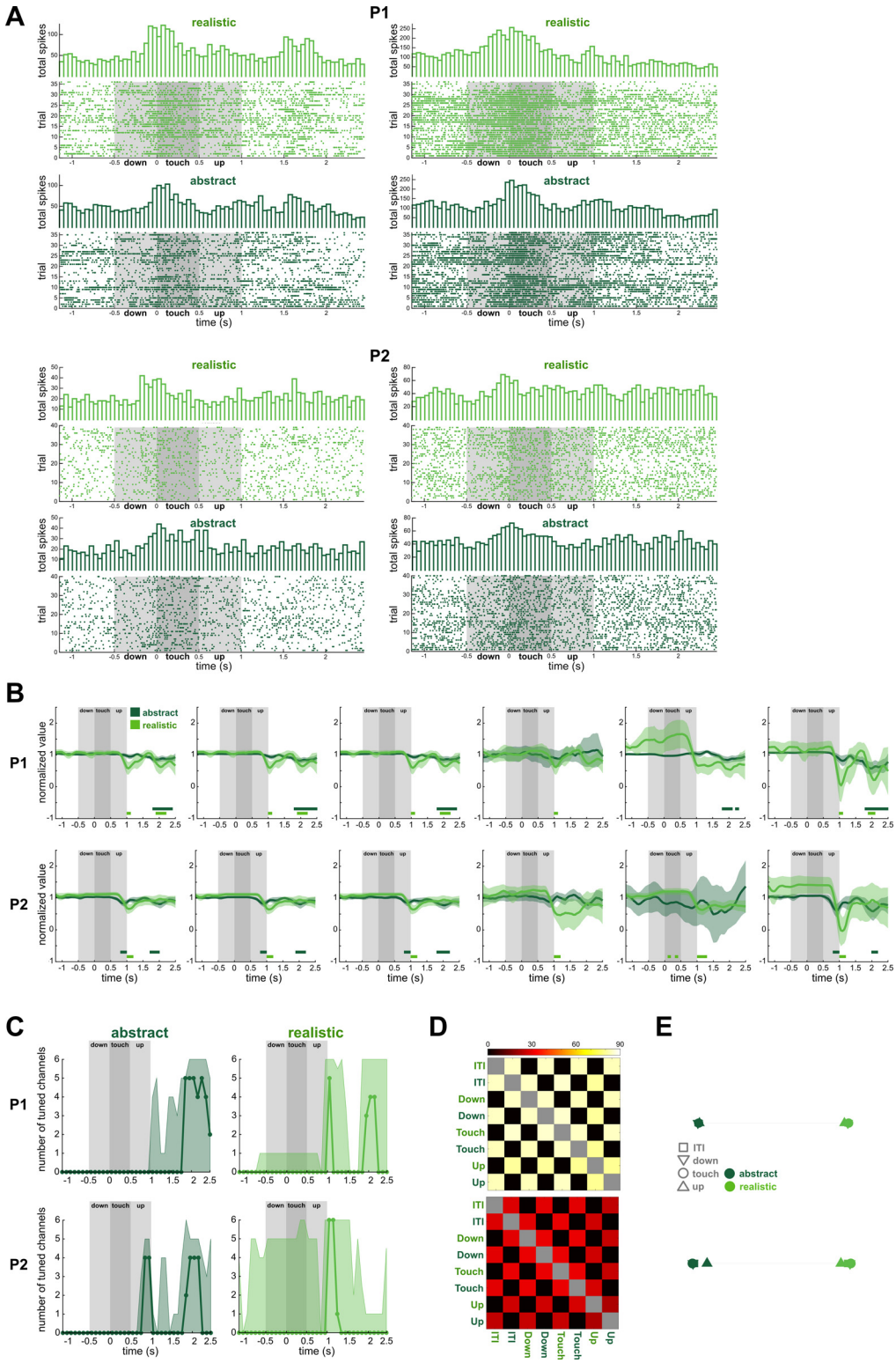

Figure A2. Raw example channel spiking activity and eye movements during catch trials. *A*: Raster plots of the example channels depicted in Fig. 5*B*, with peristimulus time histograms in 50-ms bins above each plot (*P1* $n = 36$ trials, *P2* $n = 40$). *B*: six eye movement features were recorded in each participant. The value of each feature is plotted, averaged across catch trials, by condition. Left-most three plots represent the coordinates used to encode eye position within the three-dimensional (3-D) virtual environment, and right-most three plots represent the vector of eye gaze direction. Analysis, plotting follow methods of Fig. 5*B*. *C*: percentage of features ($n = 6$) with significant modulation during catch trials relative to resting, separated by condition. Time is aligned to the onset of the "touch" phase of the visual stimulus. Shaded area indicates 95% confidence intervals (CIs) computed by bootstrapping across trials (*P1* $n = 12$ realistic, 36 abstract trials, *P2* $n = 26$ realistic, 30 abstract trials) over 1,000 iterations. Analysis, plotting follow methods of Fig. 5*A*. *D*: representational dissimilarity matrices (RDM) of eye movement features. Analysis, plotting follow methods of Fig. 5*D*. *E*: multidimensional scaling (MDS) plots of the RDMs in (*D*). Gray lines between icons are "rubber bands" whose thickness is based on the goodness of fit of the scaling (*P1*: Pearson's $r = 0.99$, $P = 2.3 \times 10^{-46}$; *P2:* $r = 0.99$, $P = 1.2 \times 10^{-31}$). Analysis, plotting follow methods of Fig. 5*E*.

DATA AVAILABILITY

Source data and supplemental videos for this study are openly available at https://doi.org/10.5281/zenodo.15284113. Code for this study is openly available at https://doi.org/10.5281/zenodo.15284865. For more resources, see Table 2.

SUPPLEMENTAL MATERIAL

Supplemental Videos S1–S3: https://doi.org/10.5281/zenodo.15284113.

ACKNOWLEDGMENTS

The authors thank the participants of this study for effort and dedication to the study, and S. Wandelt and W. Griggs for helpful discussions and insights.

GRANTS

This research was supported by the T&C Chen Brain-Machine Interface Center, the Boswell Foundation, NIH/NRSA Grant T32 NS105595, and NIH/NINDS Grant U01NS123127.

DISCLOSURES

No conflicts of interest, financial or otherwise, are declared by the authors.

AUTHOR CONTRIBUTIONS

I.A.R., L.B., D.B., and R.A.A. conceived and designed research; I.A.R., L.B., D.B., K.P., B.L., and C.L. performed experiments; I.A.R. analyzed data; I.A.R., L.B., and D.B. interpreted results of experiments; I.A.R. prepared figures; I.A.R. drafted manuscript; I.A.R., L.B., D.B., and R.A.A. edited and revised manuscript; I.A.R., L.B., D.B., K.P., B.L., C.L., and R.A.A. approved final version of manuscript.

REFERENCES

1. **Ghez C**, **Gordon J**, **Ghilardi MF.** Impairments of reaching movements in patients without proprioception. II. Effects of visual information on accuracy. *J Neurophysiol* 73: 361–372, 1995. doi:10.1152/jn.1995.73.1.361.
2. **Miall RC**, **Afanasyeva D**, **Cole JD**, **Mason P.** The role of somatosensation in automatic visuo-motor control: a comparison of congenital and acquired sensory loss. *Exp Brain Res* 239: 2043–2061, 2021. doi:10.1007/s00221-021-06110-y.
3. **Miall RC**, **Rosenthal O**, **Ørstavik K**, **Cole JD**, **Sarlegna FR.** Loss of haptic feedback impairs control of hand posture: a study in chronically deafferented individuals when grasping and lifting objects. *Exp Brain Res* 237: 2167–2184, 2019. doi:10.1007/s00221-019-05583-2.
4. **Robles-De-La-Torre G.** The importance of the sense of touch in virtual and real environments. *IEEE Multimed* 13: 24–30, 2006. doi:10.1109/MMUL.2006.69.
5. **Sainburg RL**, **Ghilardi MF**, **Poizner H**, **Ghez C.** Control of limb dynamics in normal subjects and patients without proprioception. *J Neurophysiol* 73: 820–835, 1995. doi:10.1152/jn.1995.73.2.820.
6. **Giummarra MJ**, **Gibson SJ**, **Georgiou-Karistianis N**, **Bradshaw JL.** Mechanisms underlying embodiment, disembodiment and loss of embodiment. *Neurosci Biobehav Rev* 32: 143–160, 2008. doi:10.1016/j.neubiorev.2007.07.001.
7. **Jeannerod M.** The mechanism of self-recognition in humans. *Behav Brain Res* 142: 1–15, 2003. doi:10.1016/S0166-4328(02)00384-4.
8. **Tsakiris M**, **Carpenter L**, **James D**, **Fotopoulou A.** Hands only illusion: multisensory integration elicits sense of ownership for body parts but not for non-corporeal objects. *Exp Brain Res* 204: 343–352, 2010. doi:10.1007/s00221-009-2039-3.
9. **Collinger JL**, **Wodlinger B**, **Downey JE**, **Wang W**, **Tyler-Kabara EC**, **Weber DJ**, **McMorland AJ**, **Velliste M**, **Boninger ML**, **Schwartz AB.** High-performance neuroprosthetic control by an individual with tetraplegia. *Lancet* 381: 557–564, 2013. doi:10.1016/S0140-6736(12)61816-9.
10. **Dekleva BM**, **Weiss JM**, **Boninger ML**, **Collinger JL.** Generalizable cursor click decoding using grasp-related neural transients. *J Neural Eng* 18: 2021. doi:10.1088/1741-2552/ac16b2.
11. **Moses DA**, **Metzger SL**, **Liu JR**, **Anumanchipalli GK**, **Makin JG**, **Sun PF**, **Chartier J**, **Dougherty ME**, **Liu PM**, **Abrams GM**, **Tu-Chan A**, **Ganguly K**, **Chang EF.** Neuroprosthesis for decoding speech in a paralyzed person with anarthria. *N Engl J Med* 385: 217–227, 2021. doi:10.1056/NEJMoa2027540.
12. **Armenta Salas M**, **Bashford L**, **Kellis S**, **Jafari M**, **Jo H**, **Kramer D**, **Shanfield K**, **Pejsa K**, **Lee B**, **Liu CY**, **Andersen RA.** Proprioceptive and cutaneous sensations in humans elicited by intracortical microstimulation. *eLife* 7: e32904, 2018. doi:10.7554/eLife.32904.
13. **Flesher SN**, **Collinger JL**, **Foldes ST**, **Weiss JM**, **Downey JE**, **Tyler-Kabara EC**, **Bensmaia SJ**, **Schwartz AB**, **Boninger ML**, **Gaunt RA.** Intracortical microstimulation of human somatosensory cortex. *Sci Transl Med* 8: 361ra141, 2016. doi:10.1126/scitranslmed.aaf8083.
14. **Keshtkaran MR**, **Sedler AR**, **Chowdhury RH**, **Tandon R**, **Basrai D**, **Nguyen SL**, **Sohn H**, **Jazayeri M**, **Miller LE**, **Pandarinath C.** A large-scale neural network training framework for generalized estimation of single-trial population dynamics. *Nat Methods* 19: 1572–1577, 2022. doi:10.1038/s41592-022-01675-0.
15. **Simeral JD**, **Hosman T**, **Saab J**, **Flesher SN**, **Vilela M**, **Franco B**, **Kelemen J**, **Brandman DM**, **Ciancibello JG**, **Rezaii PG**, **Eskandar EN**, **Rosler DM**, **Shenoy KV**, **Henderson JM**, **Nurmikko AV**, **Hochberg LR.** Home use of a percutaneous wireless intracortical brain-computer interface by individuals with tetraplegia. *IEEE Trans Biomed Eng* 68: 2313–2325, 2021. doi:10.1109/TBME.2021.3069119.
16. **Willsey MS**, **Nason-Tomaszewski SR**, **Ensel SR**, **Temmar H**, **Mender MJ**, **Costello JT**, **Patil PG**, **Chestek CA.** Real-time brain-machine interface in non-human primates achieves high-velocity prosthetic finger movements using a shallow feedforward neural network decoder. *Nat Commun* 13: 6899, 2022. doi:10.1038/s41467-022-34452-w.
17. **Flesher SN**, **Downey JE**, **Weiss JM**, **Hughes CL**, **Herrera AJ**, **Tyler-Kabara EC**, **Boninger ML**, **Collinger JL**, **Gaunt RA.** A brain-computer interface that evokes tactile sensations improves robotic arm control. *Science* 372: 831–836, 2021. doi:10.1126/science.abd0380.
18. **Bjånes DA**, **Bashford L**, **Pejsa K**, **Lee B**, **Liu CY**, **Andersen RA.** Multichannel intra-cortical micro-stimulation yields quick reaction times and evokes natural somatosensations in a human participant (Preprint). *medRxiv*, 2022. doi:10.1101/2022.08.08.22278389.
19. **Hughes CL**, **Flesher SN**, **Weiss JM**, **Boninger ML**, **Collinger J**, **Gaunt R.** Perception of microstimulation frequency in human somatosensory cortex. *eLife* 10: e65128, 2021. doi:10.7554/eLife.65128.
20. **Callier T**, **Brantly NW**, **Caravelli A**, **Bensmaia SJ.** The frequency of cortical microstimulation shapes artificial touch. *Proc Natl Acad Sci USA* 117: 1191–1200, 2020. doi:10.1073/pnas.1916453117.
21. **Dadarlat MC**, **O'Doherty JE**, **Sabes PN.** A learning-based approach to artificial sensory feedback leads to optimal integration. *Nat Neurosci* 18: 138–144, 2015. doi:10.1038/nn.3883.
22. **Risso G**, **Valle G.** Multisensory integration in bionics: relevance and perspectives. *Curr Phys Med Rehabil Rep* 10: 123–130, 2022. doi:10.1007/s40141-022-00350-x.
23. **Risso G**, **Valle G**, **Iberite F**, **Strauss I**, **Stieglitz T**, **Controzzi M**, **Clemente F**, **Granata G**, **Rossini PM**, **Micera S**, **Baud-Bovy G.** Optimal integration of intraneural somatosensory feedback with visual information: a single-case study. *Sci Rep* 9: 7916, 2019. doi:10.1038/s41598-019-43815-1.
24. **Caldwell DJ**, **Cronin JA**, **Wu J**, **Weaver KE**, **Ko AL**, **Rao RPN**, **Ojemann JG.** Direct stimulation of somatosensory cortex results in slower reaction times compared to peripheral touch in humans. *Sci Rep* 9: 20317, 2019. doi:10.1038/s41598-019-38619-2.
25. **Christie BP**, **Osborn LE**, **McMullen DP**, **Pawar AS**, **Thomas TM**, **Bensmaia SJ**, **Celnik PA**, **Fifer MS**, **Tenore FV.** Perceived timing of cutaneous vibration and intracortical microstimulation of human somatosensory cortex. *Brain Stimul* 15: 881–888, 2022. doi:10.1016/j.brs.2022.05.015.

26. **Godlove JM**, **Whaite EO**, **Batista AP.** Comparing temporal aspects of visual, tactile, and microstimulation feedback for motor control. *J Neural Eng* 11: 046025, 2014. doi:10.1088/1741-2560/11/4/046025.
27. **Christie BP**, **Graczyk EL**, **Charkhkar H**, **Tyler DJ**, **Triolo RJ.** Visuotactile synchrony of stimulation-induced sensation and natural somatosensation. *J Neural Eng* 16: 036025, 2019. doi:10.1088/1741-2552/ab154c.
28. **Christie BP**, **Charkhkar H**, **Shell CE**, **Marasco PD**, **Tyler DJ**, **Triolo RJ.** Visual inputs and postural manipulations affect the location of somatosensory percepts elicited by electrical stimulation. *Sci Rep* 9: 11699, 2019. doi:10.1038/s41598-019-47867-1.
29. **Pandarinath C**, **Bensmaia SJ.** The science and engineering behind sensitized brain-controlled bionic hands. *Physiol Rev* 102: 551–604, 2022. doi:10.1152/physrev.00034.2020.
30. **Gonzalez-Franco M**, **Ofek E**, **Pan Y**, **Antley A**, **Steed A**, **Spanlang B**, **Maselli A**, **Banakou D**, **Pelechano N**, **Orts-Escolano S**, **Orvalho V**, **Trutoiu L**, **Wojcik M**, **Sanchez-Vives MV**, **Bailenson J**, **Slater M**, **Lanier J.** The Rocketbox library and the utility of freely available rigged avatars. *Front Virtual Real* 1: 561558, 2020. doi:10.3389/frvir.2020.561558.
31. **Chan AW-Y**, **Baker CI.** Seeing is not feeling: posterior parietal but not somatosensory cortex engagement during touch observation. *J Neurosci* 35: 1468–1480, 2015. doi:10.1523/JNEUROSCI.3621-14.2015.
32. **Keysers C**, **Wicker B**, **Gazzola V**, **Anton J-L**, **Fogassi L**, **Gallese V.** A touching sight: SII/PV activation during the observation and experience of touch. *Neuron* 42: 335–346, 2004. doi:10.1016/S0896-6273(04)00156-4.
33. **Berg JA**, **Dammann JF 3rd**, **Tenore FV**, **Tabot GA**, **Boback JL**, **Manfredi LR**, **Peterson ML**, **Katyal KD**, **Johannes MS**, **Makhlin A**, **Wilcox R**, **Franklin RK**, **Vogelstein RJ**, **Hatsopoulos NG**, **Bensmaia SJ.** Behavioral demonstration of a somatosensory neuroprosthesis. *IEEE Trans Neural Syst Rehabil Eng* 21: 500–507, 2013. doi:10.1109/TNSRE.2013.2244616.
34. **Bekrater-Bodmann R**, **Foell J**, **Diers M**, **Kamping S**, **Rance M**, **Kirsch P**, **Trojan J**, **Fuchs X**, **Bach F**, **Çakmak HK**, **Maaß H**, **Flor H.** The importance of synchrony and temporal order of visual and tactile input for illusory limb ownership experiences—an fMRI study applying virtual reality. *PLoS One* 9: e87013, 2014. doi:10.1371/journal.pone.0087013.
35. **Costantini M**, **Robinson J**, **Migliorati D**, **Donno B**, **Ferri F**, **Northoff G.** Temporal limits on rubber hand illusion reflect individuals' temporal resolution in multisensory perception. *Cognition* 157: 39–48, 2016. doi:10.1016/j.cognition.2016.08.010.
36. **Maselli A**, **Kilteni K**, **López-Moliner J**, **Slater M.** The sense of body ownership relaxes temporal constraints for multisensory integration. *Sci Rep* 6: 30628, 2016. doi:10.1038/srep30628.
37. **Christie BP**, **Tat DM**, **Irwin ZT**, **Gilja V**, **Nuyujukian P**, **Foster JD**, **Ryu SI**, **Shenoy KV**, **Thompson DE**, **Chestek CA.** Comparison of spike sorting and thresholding of voltage waveforms for intracortical brain-machine interface performance. *J Neural Eng* 12: 016009, 2015. doi:10.1088/1741-2560/12/1/016009.
38. **Dai J**, **Zhang P**, **Sun H**, **Qiao X**, **Zhao Y**, **Ma J**, **Li S**, **Zhou J**, **Wang C.** Reliability of motor and sensory neural decoding by threshold crossings for intracortical brain–machine interface. *J Neural Eng* 16: 036011, 2019. doi:10.1088/1741-2552/ab0bfb.
39. **Zhang CY**, **Aflalo T**, **Revechkis B**, **Rosario ER**, **Ouellette D**, **Pouratian N**, **Andersen RA.** Partially mixed selectivity in human posterior parietal association cortex. *Neuron* 95: 697–708.e4, 2017. doi:10.1016/j.neuron.2017.06.040.
40. **Kriegeskorte N**, **Mur M**, **Bandettini P.** Representational similarity analysis—connecting the branches of systems neuroscience. *Front Syst Neurosci* 2: 4, 2008. doi:10.3389/neuro.06.004.2008.
41. **Nili H**, **Wingfield C**, **Walther A**, **Su L**, **Marslen-Wilson W**, **Kriegeskorte N.** A toolbox for representational similarity analysis. *PLoS Comput Biol* 10: e1003553, 2014. doi:10.1371/journal.pcbi.1003553.
42. **Walther A**, **Nili H**, **Ejaz N**, **Alink A**, **Kriegeskorte N**, **Diedrichsen J.** Reliability of dissimilarity measures for multi-voxel pattern analysis. *NeuroImage* 137: 188–200, 2016. doi:10.1016/j.neuroimage.2015.12.012.
43. **Diedrichsen J**, **Berlot E**, **Mur M**, **Schütt HH**, **Shahbazi M**, **Kriegeskorte N.** Comparing representational geometries using whitened unbiased-distance-matrix similarity. *Neurons Behav Data Anal Theory* 5: 1–31, 2021. doi:10.51628/001c.27664.
44. **Lee J**, **Maunsell JHR.** A normalization model of attentional modulation of single unit responses. *PLoS One* 4: e4651, 2009. doi:10.1371/journal.pone.0004651.
45. **Reynolds JH**, **Heeger DJ.** The normalization model of attention. *Neuron* 61: 168–185, 2009. doi:10.1016/j.neuron.2009.01.002.
46. **Tabot GA**, **Kim SS**, **Winberry JE**, **Bensmaia SJ.** Restoring tactile and proprioceptive sensation through a brain interface. *Neurobiol Dis* 83: 191–198, 2015. doi:10.1016/j.nbd.2014.08.029.
47. **Rosenthal IA**, **Bashford L**, **Kellis S**, **Pejsa K**, **Lee B**, **Liu C**, **Andersen RA.** S1 represents multisensory contexts and somatotopic locations within and outside the bounds of the cortical homunculus. *Cell Rep* 42: 112312, 2023. doi:10.1016/j.celrep.2023.112312.
48. **Lafer-Sousa R**, **Hermann KL**, **Conway BR.** Striking individual differences in color perception uncovered by 'the dress' photograph. *Curr Biol* 25: R545–R546, 2015. doi:10.1016/j.cub.2015.04.053.
49. **Ernst MO**, **Banks MS.** Humans integrate visual and haptic information in a statistically optimal fashion. *Nature* 415: 429–433, 2002. doi:10.1038/415429a.
50. **Ernst MO**, **Bülthoff HH.** Merging the senses into a robust percept. *Trends Cogn Sci* 8: 162–169, 2004. doi:10.1016/j.tics.2004.02.002.
51. **Kimura T.** Approach of visual stimuli facilitates the prediction of tactile events and suppresses beta band oscillations around the primary somatosensory area. *Neuroreport* 32: 631–635, 2021. doi:10.1097/WNR.0000000000001643.
52. **Grunewald A**, **Linden JF**, **Andersen RA.** Responses to auditory stimuli in macaque lateral intraparietal area. I. Effects of training. *J Neurophysiol* 82: 330–342, 1999. doi:10.1152/jn.1999.82.1.330.
53. **Linden JF**, **Grunewald A**, **Andersen RA.** Responses to auditory stimuli in macaque lateral intraparietal area. II. Behavioral modulation. *J Neurophysiol* 82: 343–358, 1999. doi:10.1152/jn.1999.82.1.343.
54. **Dionne JK**, **Legon W**, **Staines WR.** Crossmodal influences on early somatosensory processing: interaction of vision, touch, and task-relevance. *Exp Brain Res* 226: 503–512, 2013. doi:10.1007/s00221-013-3462-z.
55. **Blakemore S-J**, **Bristow D**, **Bird G**, **Frith C**, **Ward J.** Somatosensory activations during the observation of touch and a case of vision–touch synaesthesia. *Brain* 128: 1571–1583, 2005. doi:10.1093/brain/awh500.
56. **Bufalari I**, **Aprile T**, **Avenanti A**, **Di Russo F**, **Aglioti SM.** Empathy for pain and touch in the human somatosensory cortex. *Cereb Cortex* 17: 2553–2561, 2007. doi:10.1093/cercor/bhl161.
57. **Ebisch SJH**, **Perrucci MG**, **Ferretti A**, **Del Gratta C**, **Romani GL**, **Gallese V.** The sense of touch: Embodied simulation in a visuotactile mirroring mechanism for observed animate or inanimate touch. *J Cogn Neurosci* 20: 1611–1623, 2008. doi:10.1162/jocn.2008.20111.
58. **Kuehn E**, **Haggard P**, **Villringer A**, **Pleger B**, **Sereno MI.** Visually-driven maps in Area 3b. *J Neurosci* 38: 1295–1310, 2018. doi:10.1523/JNEUROSCI.0491-17.2017.
59. **Kuehn E**, **Trampel R**, **Mueller K**, **Turner R**, **Schütz-Bosbach S.** Judging roughness by sight-A 7-tesla fMRI study on responsivity of the primary somatosensory cortex during observed touch of self and others. *Hum Brain Mapp* 34: 1882–1895, 2013. doi:10.1002/hbm.22031.
60. **Longo MR**, **Pernigo S**, **Haggard P.** Vision of the body modulates processing in primary somatosensory cortex. *Neurosci Lett* 489: 159–163, 2011. doi:10.1016/j.neulet.2010.12.007.
61. **Schaefer M**, **Xu B**, **Flor H**, **Cohen LG.** Effects of different viewing perspectives on somatosensory activations during observation of touch. *Hum Brain Mapp* 30: 2722–2730, 2009. doi:10.1002/hbm.20701.
62. **Morrison I**, **Lloyd D**, **Di Pellegrino G**, **Roberts N.** Vicarious responses to pain in anterior cingulate cortex: is empathy a multisensory issue? *Cogn Affect Behav Neurosci* 4: 270–278, 2004. doi:10.3758/CABN.4.2.270.
63. **Espenhahn S**, **Yan T**, **Beltrano W**, **Kaur S**, **Godfrey K**, **Cortese F**, **Bray S**, **Harris AD.** The effect of movie-watching on electroencephalographic responses to tactile stimulation. *Neuroimage* 220: 117130, 2020. doi:10.1016/j.neuroimage.2020.117130.
64. **Chapman CE**, **Meftah E-M.** Independent controls of attentional influences in primary and secondary somatosensory cortex. *J Neurophysiol* 94: 4094–4107, 2005. doi:10.1152/jn.00303.2005.
65. **Popovich C**, **Staines WR.** The attentional-relevance and temporal dynamics of visual-tactile crossmodal interactions differentially

influence early stages of somatosensory processing. *Brain Behav* 4: 247–260, 2014. doi:10.1002/brb3.210.

66. **Colino FL**, **Lee J-H**, **Binsted G.** Availability of vision and tactile gating: vision enhances tactile sensitivity. *Exp Brain Res* 235: 341–348, 2017. doi:10.1007/s00221-016-4785-3.
67. **Haggard P**, **Christakou A**, **Serino A.** Viewing the body modulates tactile receptive fields. *Exp Brain Res* 180: 187–193, 2007. doi:10.1007/s00221-007-0971-7.
68. **Kennett S**, **Taylor-Clarke M**, **Haggard P.** Noninformative vision improves the spatial resolution of touch in humans. *Curr Biol* 11: 1188–1191, 2001. doi:10.1016/S0960-9822(01)00327-X.
69. **Press C**, **Taylor-Clarke M**, **Kennett S**, **Haggard P.** Visual enhancement of touch in spatial body representation. *Exp Brain Res* 154: 238–245, 2004. doi:10.1007/s00221-003-1651-x.
70. **Tipper S**, **Phillips N**, **Dancer C**, **Lloyd D**, **Howard L**, **McGlone F.** Vision influences tactile perception at body sites that cannot be viewed directly. *Exp Brain Res* 139: 160–167, 2001. doi:10.1007/s002210100743.
71. **Ariani G**, **Pruszynski JA**, **Diedrichsen J.** Motor planning brings human primary somatosensory cortex into action-specific preparatory states. *eLife* 11: e69517, 2022. doi:10.7554/eLife.69517.
72. **Bashford L**, **Rosenthal I**, **Kellis S**, **Pejsa K**, **Kramer D**, **Lee B**, **Liu C**, **Andersen RA.** The neurophysiological representation of imagined somatosensory percepts in human cortex. *J Neurosci* 41: 2177–2185, 2021. doi:10.1523/JNEUROSCI.2460-20.2021.
73. **Gale DJ**, **Flanagan JR**, **Gallivan JP.** Human somatosensory cortex is modulated during motor planning. *J Neurosci* 41: 5909–5922, 2021. doi:10.1523/JNEUROSCI.0342-21.2021.
74. **Yoo S-S**, **Freeman DK**, **McCarthy JJ**, **Jolesz FA.** Neural substrates of tactile imagery: a functional MRI study. *Neuroreport* 14: 581–585, 2003. doi:10.1097/00001756-200303240-00011.
75. **Jafari M**, **Aflalo T**, **Chivukula S**, **Kellis SS**, **Salas MA**, **Norman SL**, **Pejsa K**, **Liu CY**, **Andersen RA.** The human primary somatosensory cortex encodes imagined movement in the absence of sensory information. *Commun Biol* 3: 757, 2020. doi:10.1038/s42003-020-01484-1.
76. **Klaes C**, **Shi Y**, **Kellis S**, **Minxha J**, **Revechkis B**, **Andersen RA.** A cognitive neuroprosthetic that uses cortical stimulation for somatosensory feedback. *J Neural Eng* 11: 056024, 2014. doi:10.1088/1741-2560/11/5/056024.
77. **Hughes CL**, **Flesher SN**, **Gaunt RA.** Effects of stimulus pulse rate on somatosensory adaptation in the human cortex. *Brain Stimul* 15: 987–995, 2022. doi:10.1016/j.brs.2022.05.021.